NIST Interagency Report
NIST IR 8570

Refrigerant Properties Development R&D

Final Report to U.S. Department of Energy on Interagency Agreements 892434-19-S-EE000031 and 892434-23-S-EE000120

Mark O. McLinden
Katrina N. Avery
Ala Bazyleva
Ian H. Bell
Tara J. Fortin
Marcia L. Huber
Andrei F. Kazakov
Eric W. Lemmon
Stephanie L. Outcalt
Richard A. Perkins
Elizabeth G. Rasmussen
Demian Riccardi
Aaron J. Rowane

This publication is available free of charge from:
https://doi.org/10.6028/NIST.IR.8570

NIST NATIONAL INSTITUTE OF STANDARDS AND TECHNOLOGY
U.S. DEPARTMENT OF COMMERCE

NIST Interagency Report
NIST IR 8570

Refrigerant Properties Development R&D

Final Report to U.S. Department of Energy on Interagency Agreements 892434-19-S-EE000031 and 892434-23-S-EE000120

Mark O. McLinden
Katrina N. Avery
Ala Bazyleva
Ian H. Bell*
Tara J. Fortin
Marcia L. Huber
Andrei F. Kazakov
Eric W. Lemmon
Stephanie L. Outcalt*
Richard A. Perkins*
Elizabeth G. Rasmussen*
Demian Riccardi
Aaron J. Rowane
Applied Chemicals and Materials Division
Material Measurement Laboratory

**Former or retired NIST employee;*
all work for this publication was done while at NIST.

This publication is available free of charge from:
https://doi.org/10.6028/NIST.IR.8570

March 2025

U.S. Department of Commerce
Howard Lutnick, Secretary of Commerce

National Institute of Standards and Technology
Craig Burkhardt, Acting Under Secretary of Commerce for Standards and Technology and Acting NIST Director

NIST IR 8570
March 2025

Certain equipment, instruments, software, or materials, commercial or non-commercial, are identified in this paper in order to specify the experimental procedure adequately. Such identification does not imply recommendation or endorsement of any product or service by NIST, nor does it imply that the materials or equipment identified are necessarily the best available for the purpose.

NIST Technical Series Policies
Copyright, Use, and Licensing Statements
NIST Technical Series Publication Identifier Syntax

Publication History
Approved by the NIST Editorial Review Board on 2025-03-25

How to Cite this NIST Technical Series Publication
McLinden, M.O., Avery, K.N., Bazyleva, A., Bell, I.A., Fortin, T.J., Huber, M.L., Kazakov, A.F., Lemmon, E.W., Outcalt, S.L., Perkins, R.A., Riccardi, D., Rasmussen, E.G., Rowane, A.J. (2025), Refrigerants Properties Development R&D: Final Report to U.S. Department of Energy on Interagency Agreements 892434-19-S-EE000031 and 892434-23-S-EE000120. (National Institute of Standards and Technology, Gaithersburg, MD), NIST Interagency Report (IR) NIST IR 8570. https://doi.org/10.6028/NIST.IR.8570.

Author ORCID IDs

McLinden, M.O.:	0000-0002-1082-309X
Avery, K.N.:	0009-0005-9707-2098
Bazyleva, A:	0000-0003-3018-2020
Bell, I.H.:	0000-0003-1091-9080
Fortin, T.J.:	0000-0001-6150-8930
Huber, M.L.:	0000-0002-7976-741X
Kazakov, A.F.	0009-0008-6964-3086
Lemmon, E.W.	0000-0002-0974-0203
Outcalt, S.L.:	0000-0001-8143-7316
Perkins, R.A.:	0000-0002-8526-6742
Rasmussen, E.G.:	0000-0003-2871-6599
Riccardi, D.:	0000-0001-8095-7803
Rowane, A.J.:	0000-0001-7605-0774

Contact Information
mark.mclinden@nist.gov

Abstract

The HVAC&R industry is facing the challenge of phasing down the use of the HFC (hydrofluoro-carbon) refrigerants. New energy-efficient refrigerants are required, and accurate property data for them are needed to design and operate new HVAC equipment using the new refrigerants.

The present work has measured property data on key mixtures among the olefins R-1234yf, R-1234ze(E), R-1130(E), R-1132a, R-1132(E), and R-1336mzz(Z), together with the HFCs R-152a, R-32, and R-227ea. Measurements were also carried out on pure R-1130(E). Included were vapor-liquid equilibrium (VLE) measurements, pressure-density-temperature-composition (p, ρ, T, x) data, and speed of sound. This report summarizes the measurements carried out, describes the experimental techniques used, and gives examples of the results.

These data were then used to develop models of the thermodynamic properties; these are expressed in terms of “equations of state” (EOS). In addition to the mixture models, EOS are presented for pure R-1130(E) and R-1132(E). The main output of the project takes the form of the numerical parameters for the pure-fluid and mixture models, which are reported here and in the form of data files for use with the NIST REFPROP database of refrigerant properties.

Full details of both the experimental and modeling efforts are given in papers published in archival journals, which are linked in the report. The present work has added important new refrigerants and refrigerant blends to the existing data set. As a result, industry is able to evaluate a wider range of options.

Keywords

equation of state; measurements; mixtures; refrigerants; thermodynamic properties

Table of Contents

List of Tables

List of Figures

Acknowledgments

This material is based upon work supported by the U.S. Department of Energy's Office of Energy Efficiency and Renewable Energy (EERE) Building Technologies Office (BTO) under agreements 892434-19-S-EE000031 and 892434-23-S-EE000120. It was carried out in coordination with the Air-Conditioning, Heating, and Refrigeration Technology Institute under DOE Award DE-EE0008406.

Disclaimer

This report was prepared as an account of work sponsored by an agency of the United States Government. Neither the United States Government nor any agency thereof, nor any of their employees, makes any warranty, express or implied, or assumes any legal liability or responsibility for the accuracy, completeness, or usefulness of any information, apparatus, product, or process disclosed, or represents that its use would not infringe privately owned rights. Reference herein to any specific commercial product, process, or service by trade name, trademark, manufacturer, or otherwise does not necessarily constitute or imply its endorsement, recommendation, or favoring by the United States Government or any agency thereof. The views and opinions of authors expressed herein do not necessarily state or reflect those of the United States Government or any agency thereof.

Executive Summary

Improvements in the efficiency of building equipment play an important role in achieving U.S. energy security. Presently, the HVAC&R (heating, refrigeration, air-conditioning, and refrigeration) industry is facing the challenge of phasing down the use of the HFC (hydrofluorocarbon) refrigerants, which it has used over the past decades. New energy-efficient refrigerants are needed, and accurate property data for them are required to design and operate new HVAC equipment using the new refrigerants. This project provides such data. The focus was on refrigerant blends because previous work revealed few pure fluids with the necessary combination of safety, performance, and environmental characteristics.

The present work has measured and modeled property data on key mixtures among the olefins R-1234yf, R-1234ze(E), R-1130(E), R-1132a, R-1132(E), and R-1336mzz(Z), together with the HFCs R-152a, R-32, and R-227ea. Measurements were also carried out on pure R-1130(E), and models for the pure fluids R-1130(E) and R-1132(E) were developed.

Experimental efforts included vapor-liquid equilibrium (VLE) measurements, pressure-density-temperature-composition (p, ρ, T, x) data, and speed of sound. The measurements were selected to provide an optimal data set for the purposes of fitting property models. This report summarizes the measurements carried out, describes the experimental techniques used, and gives examples of the results.

These data were then used to develop models of the thermodynamic properties; these are expressed in terms of “equations of state” (EOS), which are mathematical models representing all thermodynamic properties of a pure fluid or blend. It is through these EOS that the property data are made available to engineers in industry for the purposes of cycle analysis, heat transfer analysis, equipment design, and the analysis of system tests. The refrigerants and blends studied in this work were decided in cooperation with an industry working group convened by the Air-Conditioning, Heating and Refrigeration Technology Institute (AHRTI), ensuring that the results would be relevant to the industry.

Full details of both the experimental and modeling efforts are given in papers published in archival journals, which are linked in the report. The main result of the project takes the form of the numerical parameters for the pure-fluid and mixture models, which are reported here and in the form of data files for use with the NIST REFPROP database of refrigerant properties. Note that these results have been periodically released over the course of the project making interim results available to the industry.

The present work has added important new refrigerants and refrigerant blends to the existing data set. Conducting the work at a NIST group specializing in properties was much more cost effective than scattered efforts at individual companies investigating specific mixtures. The methods employed were state of the art, generating highly accurate data and models. As a result, industry is able to evaluate a wider range of options. The public will thus benefit from more efficient refrigeration and air-conditioning equipment.

1. Background

Building equipment efficiency improvements play an important role in achieving U.S. energy security. According to recent Energy Information Administration (EIA) estimates [1] residential and commercial buildings will consume 37.85 quads (3.99×10^{19} J) or 38.6 % of the total US primary energy consumption in the year 2030, continuing to exceed the energy consumption of the industrial and transportation sectors.

In 2014, the United States, Canada, and Mexico proposed an amendment to the Montreal Protocol to reduce production and consumption of hydrofluorocarbon (HFC) refrigerants by 85 % during the period 2016–2035, for Non-A5 (developed) countries. Under the proposal, A5 (developing) countries would reduce HFC production and consumption by 85 % during the later period 2025–2045. This proposal (with small modifications) was formally adopted as the Kigali Amendment to the Montreal Protocol in October 2016;[2] it entered into force on January 1, 2019 and was implemented in the U.S. as part of the American Innovation and Manufacturing Act of 2020.[3] Reducing the nation's HFC consumption by 85 percent will require an enormous, but possible, deviation from business-as-usual activity in the HVAC&R industry. This deviation requires the development of new HVAC solutions, including new refrigerants as the phase-down targets become progressively more difficult each year. The present project would put resources in place to help enable this transition.

To meet these goals, new energy-efficient refrigerants are needed. Accurate property data and correlations are needed to design and operate new HVAC equipment using them.

The simulation of cycle performance and the analysis of laboratory measurements in equipment require thermodynamic properties of the considered refrigerant. The thermodynamic properties are expressed in terms of an “equation of state” or EOS which is a mathematical model representing all thermodynamic properties of a pure fluid or blend. The properties of a refrigerant blend are given by a combination of the EOS of the constituent pure fluids in the blend plus additional terms representing the mixture.

Any equation of state (for a pure fluid or mixture) requires experimental data to fit adjustable parameters and validate its accuracy. While pure-fluid EOS are available and generally adequate for the new refrigerants, this is not the case for refrigerant blends. This task has carried out the measurements necessary to define the mixture terms in the EOS models. These terms are expressed in terms of binary pairs of components; a mixture of the components A, B, and C, for example, is expressed in terms of the binary pairs A/B, A/C, and B/C. Thus, the present measurements were carried out on binary mixtures, even though ternary (three-component) or higher mixtures are also of interest. The mixture parameters used to date were often based on limited experimental data from the literature or, in some cases, were entirely predicted, and this project will improve the data situation.

2. Project Objectives

The overall objective of this project was to support the Building Technologies Office goal for 50 % energy savings by 2030 and comply with the Multi-Year Program Plan.

NIST partnered with AHRTI and Oak Ridge National Laboratory (ORNL), in a broader research effort focused on the heat transfer performance and compatibility aspects of new refrigerant technology in addition to the thermodynamic properties research at NIST. This effort consisted of multiple tasks addressing specific research needs that were ranked as high-priority activities in the DOE roadmap.

The main goal of the NIST effort was to overcome the hurdles of implementing environmentally friendly and energy-efficient refrigerants in HVACR products by providing accurate refrigerant properties data and correlations. The outcome of the effort was a list of measured refrigerant properties, which NIST then used to develop thermodynamic models for mixtures containing the new refrigerants with an emphasis on the hydrofluoroolefins, HFOs. The resulting models were then implemented in the NIST REFPROP database.[4]

Experimental data on key binary pairs among the olefins R-1234yf, R-1234ze(E), R-1130(E), R-1132a, R-1132(E), and R-1336mzz(Z), together with the HFCs R-152a, R-32, and R-227ea, were generated. Some of the basic properties of these fluids are given in Table 2-1 and ball-and-stick representations of their molecular structures are shown in Fig. 2-1. The measured data were used to develop the mixture property models that would enable accurate cycle modeling and equipment design. AHRTI set up an industrial working group, and the measurements were carried out on blends selected according to the priorities of the working group. The measurements consisted of vapor-liquid equilibria (VLE or bubble-point pressure), liquid-phase speed of sound, and pressure-density-temperature measurements in the liquid, vapor, and supercritical states; these are summarized in Tables 2-2 and 2-3.

The present work was coordinated with a parallel and complementary effort at NIST funded by the U.S. Department of Defense under SERDP (Strategic Environmental Research and Development Program). That work focused on replacements for R-134a and included thermodynamic property measurements on the blends R-1234yf/134a, R-134a/1234ze(E), R-1234yf/1234ze(E), R-125/1234yf, R-1234yf/152a, and R-1234ze(E)/227ea. In addition to the property measurements, the project also considered flammability of the blends and included heat transfer studies and testing in equipment. The results of the SERDP project were published as a NIST report [5] and in journal papers, which are referenced in Sec. 7. Although separate, the working group was kept abreast of the planned work and results of the SERDP project so that there was not duplication of effort. In some cases, blends identified by the working group as being of high interest were already included in the SERDP project, but only for limited measurements; thus, further measurements were carried out with DOE funding, as indicated in Table 2-2.

Table 2-1. Refrigerants considered in this work.

R-number	IUPAC name	Structure	T_{boil}/˚C	T_{crit}/˚C	MW
Olefins					
R-1132a	1,1-difluoroethene	$CF_2=CH_2$	-82.81	29.66	64.035
R-1132(E)	*trans*-1,2-difluoroethene	(E) CHF=CHF	-52.64	75.67	64.035
R-1234yf	2,3,3,3-tetrafluoropropene	$CH_2=CFCF_3$	-29.46	94.70	114.042
R-1234ze(E)	*trans*-1,3,3,3-tetrafluoropropene	(E) $CHF=CHCF_3$	-18.97	109.36	114.042
R-1336mzz(Z)	*cis*-1,1,1,4,4,4-hexafluorobutene	(Z) $CF_3CH=CHCF_3$	33.45	171.35	164.056
R-1130(E)	*trans*-1,2-dichloroethene	(E) ClHC=CHCl	47.22	242.54	96.943
HFCs					
R-32	difluoromethane	CH_2F_2	-51.65	78.11	52.024
R-152a	1,1-difluoroethane	CHF_2CH_3	-24.02	113.26	66.051
R-227ea	1,1,1,2,3,3,3-heptafluoropropane	CF_3CHFCF_3	-16.34	101.75	170.029

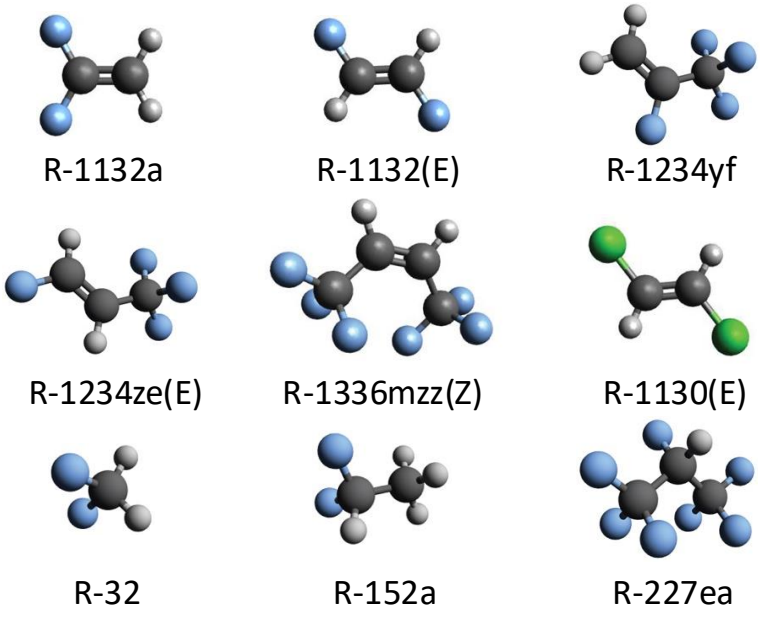

Fig. 2-1. Molecular representations of refrigerants considered in this work; carbon atoms are black, hydrogen gray, fluorine blue, and chlorine green.

Table 2-2. Summary of the measurements and modeling carried out in Phase I of the project (budget periods 1 and 2); measurements carried out with SERDP funding are listed in italics.

Measurements			Modeling
(p, ρ, T, x)	Speed of sound (liquid)	VLE	Mixture model
R-32/1234yf	R-32/1234yf	R-32/1234yf	R-32/1234yf
R-32/1234ze(E)	R-32/1234ze(E)	R-32/1234ze(E)	R-32/1234ze(E)
R-152a/1234yf	R-152a/1234yf	*R-152a/1234yf* [(a)]	R-152a/1234yf
	R-125/1234yf	*R-125/1234yf* [(a)]	R-125/1234yf
R-1234ze(E)/227ea	R-1234ze(E)/227ea	*R-1234ze(E)/227ea* [(a)]	R-1234ze(E)/227ea
	R-1132a (pure)	R-1132a/1234yf	R-1132a/1234yf

[(a)]Measurements carried out with SERDP funding.

Table 2-3. Summary of the measurements and modeling carried out in Phase II of the project (budget period 3).

Measurements			**Modeling**	
(p, ρ, T, x)	Speed of sound (liquid)	VLE/ (p_{sat} for pures)	Pure-fluid EOS	Mixture model
R-1132(E)/ 1234yf	R-1132(E)/ 1234yf			R-1132(E)/ 1234yf
R-1132(E)/32	R-1132(E)/32		R-1132(E)	R-1132(E)/32
R-1130(E)	R-1130(E)	R-1130(E)	R-1130(E)	
	R-1336mzz(Z)/ 1130(E)	R-1336mzz(Z)/ 1130(E)		R-1336mzz(Z)/ 1130(E)
		R-1336mzz(Z)		

3. Project Results—Experimental Property Measurements

Measurements carried out in the current project included vapor-liquid equilibrium (VLE) measurements, pressure-density-temperature-composition (p, ρ, T, x) data in the single-phase and supercritical regions, and speed of sound in the single-phase liquid region. For most blends, measurements were carried out at nominal compositions of (0.33/0.67) and (0.67/0.33) mole fraction. These measurements allowed fitting mixture EOS models. The measurements are summarized in Tables 3-1 and 3-2. The remainder of this section provides an overview of the measurement methods and results, with details given in the published papers linked in Sec. 7.

Table 3-1. Refrigerant blend properties measured in Phase I of the project.

Blend	Composition (mole frac)	T-range (K)	p-range (MPa)	Number of points[a]
Vapor-Liquid Equilibria (VLE)				
R-32/1234yf	(0.3686/0.6314)	270 – 350	0.52 – 3.66	9
R-32/1234yf	(0.6881/0.3119)	270 – 345	0.65 – 4.28	9
R-32/1234ze(E)	(0.3409/0.6591)	270 – 360	0.40 – 3.59	10
R-32/1234ze(E)	(0.6455/0.3545)	270 – 350	0.56 – 4.12	10
R-1132a/1234yf	(0.4012/0.5988)	270 – 325	0.90 – 2.94	13
R-1132a/1234yf	(0.7063/0.2937)	270 – 310	1.43 – 3.40	9
Speed of Sound—Liquid Phase				
R-125/1234yf	(0.3335/0.6665)	230 – 345	0.10 – 13.8	69
R-125/1234yf	(0.6664/0.3336)	230 – 345	0.47 – 21.5	64
R-1234yf/152a	(0.3334/0.6666)	235 – 345	0.26 – 14.1	69
R-1234yf/152a	(0.6653/0.3347)	230 – 345	0.14 – 11.1	69
R-1234ze(E)/227ea	(0.3327/0.6673)	230 – 345	0.37 – 48.6	158
R-1234ze(E)/227ea	(0.6680/0.3320)	230 – 335	0.05 – 48.0	155
R-32/1234yf	(0.3381/0.6619)	230 – 345	0.16 – 11.4	64
R-32/1234yf	(0.6721/0.3279)	230 – 345	1.34 – 12.5	30
R-32/1234ze(E)	(0.3351/0.6649)	230 – 345	0.73 – 52.5	189
R-32/1234ze(E)	(0.6667/0.3333)	230 – 345	0.21 – 51.5	142
R-1132a/propane[b]	(0.9726/0.0274)	230 – 345	1.40 – 49.1	84
R-1132a/propane	(0.9492/0.0508)	230 – 345	1.34 – 47.2	83
R-1132a/propane	(0.9113/0.0887)	230 – 345	0.67 – 49.2	99

[a]Distinct (T, p, x) state points; multiple replicate measurements were made at most state points.

[b]Measurements on pure R-1132a were not possible, and R-1132a/propane data were used to extrapolate results to the pure R-1132a (see Sec. 3.4).

Table 3-1 (continued). Refrigerant blend properties measured in Phase I of the project.

Blend	Composition (mole frac)	*T*-range (K)	*p*-range (MPa)	Number of points[a]
(p, ρ, T, x)—Liquid and Vapor Phases and Supercritical States				
R-32/1234yf	(0.3368/0.6632)	230 – 400	0.09 – 9.70	112
R-32/1234yf	(0.6721/0.3279)	230 – 400	0.12 – 14.1	105
R-32/1234ze(E)	(0.3351/0.6649)	230 – 400	0.14 – 19.5	132
R-32/1234ze(E)	(0.6667/0.3333)	230 – 400	0.15 – 22.1	105
R-1234yf/152a	(0.3334/0.6666)	230 – 400	0.08 – 11.8	81
R-1234yf/152a	(0.6653/0.3347)	230 – 400	0.08 – 10.5	84
R-1234ze(E)/227ea	(0.3327/0.6673)	230 – 400	0.10 – 17.1	80
R-1234ze(E)/227ea	(0.6680/0.3320)	230 – 400	0.10 – 17.1	84

[a]Distinct (*T*, *p, x*) state points; multiple replicate measurements were made at most state points.

Table 3-2. Refrigerant blend properties measured in Phase II of the project.

Blend/Pure Fluid	Composition (mole frac)	*T*-range (K)	*p*-range (MPa)	Number of points[a]
Vapor-Liquid Equilibria (VLE)/(Vapor Pressure for Pures)				
R-1336mzz(Z)/1130(E)	(0.466/0.534)	265 – 360	0.020 – 0.54	19
R-1336mzz(Z)/1130(E)	(0.748/0.252)	265 – 360	0.020 – 0.57	21
R-1336mzz(Z)/1130(E)	(0.768/0.232)	265 – 360	0.020 – 0.56	20
R-1336mzz(Z)	–	265 – 360	0.017 – 0.52	19
R-1130(E)	–	265 – 360	0.010 – 0.33	20
Speed of Sound—Liquid Phase				
R-1132(E)/1234yf	(0.435/0.565)	230 – 342	0.66 – 8.00	173
R-1132(E)/32	(0.336/0.664)	230 – 325	1.59 – 8.21	137
R-1336mzz(Z)/1130(E)	(0.634/0.365)	240 – 420	0.17 – 25.7	86
R-1130(E)	–	230 – 420	0.43 – 26.7	145
(p, ρ, T, x)—Liquid Phase				
R-1132(E)/1234yf	(0.435/0.565)	261 – 336	0.39 – 7.1	58
R-1132(E)/32	(0.336/0.664)	264 – 334	1.8 – 6.6	65
R-1130(E)	–	270 – 410	0.50 – 30.0	136

[a]Distinct (*T*, *p, x*) state points; multiple replicate measurements were made at most state points.

3.1. VLE (Vapor Pressure)

The measurement of vapor-liquid equilibrium is the mixture analog of vapor pressure for a pure component. VLE data are the most important type of data needed for fitting a mixture EOS. They indicate, for example, the departure from ideal behavior and the presence or absence of azeotropes. Measurements of the bubble-point pressure as a function of temperature and liquid-phase composition (p, T, x) were made here. This instrument was also used to measure pure-fluid vapor pressure—either as a project deliverable in the case of R-1130(E) or to validate performance of the instrument in the case of R-1336mzz(Z), which has a well-known vapor pressure. Conceptually, the measurement is very simple: load a liquid sample of known composition into a closed volume (i.e., "measuring cell"), bring the measuring cell to some temperature, and when the temperature has stabilized, measure the pressure.

A schematic of the instrument used to make the measurements is shown in Fig. 3-1; it is an updated version of the instrument described by Outcalt and Lemmon.[6] The heart of the instrument was a cylindrical stainless steel measuring cell with a sapphire window on each end so that the liquid level in the cell was visible. The cell had an internal volume of approximately 30 mL. The operating range of the apparatus was 265 K to 360 K, with pressures to 7 MPa.

The cell was fitted inside a temperature-controlled, insulated aluminum block. The valves for filling the system were installed in the aluminum block to limit the sample volume outside the temperature-controlled zone. Cooling fluid from an external refrigerated circulator flowed through channels drilled into the aluminum block. Cartridge heaters installed in the aluminum block provided heat for operation above ambient temperature. Thin-film type heaters were adhered to the outside of the block for fine control of the temperature. Temperature control was automated with the modified PID algorithm of Hust et al.[7]

Temperature was measured with a standard platinum resistance thermometer (SPRT) installed in a thermowell adjacent to the measuring cell. The pressure was measured with one of two oscillating-quartz-crystal pressure transducers connected to the system through one of the ports at the top of the cell. These transducers had full-scale ranges of 0.7 MPa and 7.0 MPa; the low-range transducer had the higher sensitivity, and it was used whenever possible. The transducers were housed in separate thermostats maintained at 313 K.

For loading, the sample bottle was connected to the system in an inverted position so that the liquid phase was loaded into the cell. Prior to loading a sample into the system, the system was evacuated and cooled to approximately 270 K, and the pressure reading under vacuum was recorded. The sample was then quickly loaded into the system until only a small vapor space remained in the equilibrium cell. Stirring of the sample was effected by a stir bar inside the cell that was magnetically coupled to an external motor.

By loading the sample from the liquid phase of the sample bottle and filling the measuring cell nearly full, the liquid-phase composition in the cell was nearly that of the bulk composition of the sample bottle. Small corrections to the composition were made using the mixture model in REFPROP and assuming equilibrium between the liquid and vapor phases in both the sample bottle and measuring cell.

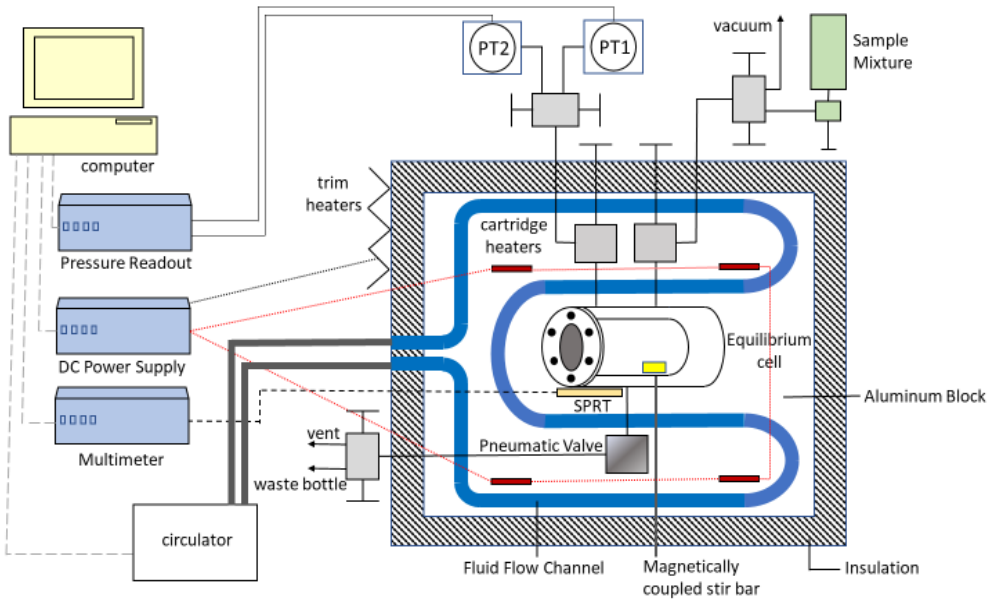

Fig. 3-1. Schematic of instrument for vapor-liquid equilibria measurements. Main components include a stainless steel equilibrium cell housed in a thermostated aluminum block, standard platinum resistance thermometer (SPRT), and two oscillating quartz crystal pressure transducers (PT1 and PT2) with maximum pressure ranges of 0.7 MPa and 7 MPa.

Measurements commenced at 270 K. After temperature and pressure equilibrium were obtained, the conditions were recorded. The temperature was then increased by an increment of 5 K or 10 K. As the temperature was increased, the liquid expanded, eventually filling the cell with compressed liquid. As a result, it was necessary to periodically release a small amount of liquid from the bottom of the cell to maintain a vapor space; this was done by opening a pneumatically actuated valve. Repeat measurements were conducted at a minimum of two temperatures. These repeats established the repeatability of the measurements and also helped to determine whether the loss of small amounts of the liquid phase affected the sample composition to the extent that duplicate measurements at a given temperature yielded different bubble-point pressures. In almost all instances this was not the case.

The principal sources of uncertainty in these measurements arose from the measurements of temperature, pressure, and sample composition as well as repeatability of the measurements. The SPRT was calibrated with fixed-point cells, and the standard (k = 1) uncertainty in temperature, including calibration, repeatability and possible temperature gradients was estimated to be 20 mK. The pressure transducers were calibrated with a piston gage, and the zero of the transducers was regularly checked. The uncertainty in the pressure was 0.005 % of the full-scale pressure (i.e., 0.035 kPa or 0.35 kPa for the two transducers). As described in Sec. 3.5, the uncertainty in the composition due to the weighings was less than 0.0001 mole fraction. Because of the two-phase nature of the liquid-phase samples and because the weighings could determine only the overall (bulk) composition of the sample, it was necessary

to estimate the change in composition caused by the liquid/vapor fractionation inside the cylinder. This change was less than 0.0005 mole fraction, and its standard uncertainty was estimated to be less than 0.0001 mole fraction. Thus, the combined, expanded uncertainty in composition of the liquid-phase samples was estimated to be less than 0.00028 mole fraction. In addition to these uncertainties, the standard deviation in repeat measurements were added in quadrature to arrive at the overall uncertainty, which is stated in the tables of VLE data presented in the published papers linked in Sec. 7.

For all of the property measurements presented here, deviations of the experimental data from the models developed in this project are expressed as relative deviations:

$$\Delta z = 100 \cdot \frac{\left(z_{\text{exp}} - z_{\text{EOS}}\right)}{z_{\text{EOS}}} \tag{3-1}$$

where Δz is the relative deviation, z_{exp} is a measured property, and z_{EOS} is the value predicted by the model.

An example of the VLE measurements for the blend of R-1336mzz(Z) and R-1130(E) is shown in Fig. 3-2. The left panel shows the measured points plotted as pressure over a temperature range of 265 K to 360 K; note that for this blend the pure components were also measured. The right panel plots the pressure as a function of composition for temperatures of 300 K and 320 K; the maximum in the pressure indicates the existence of an azeotrope at 0.6 mole fraction R-1336mzz(Z).

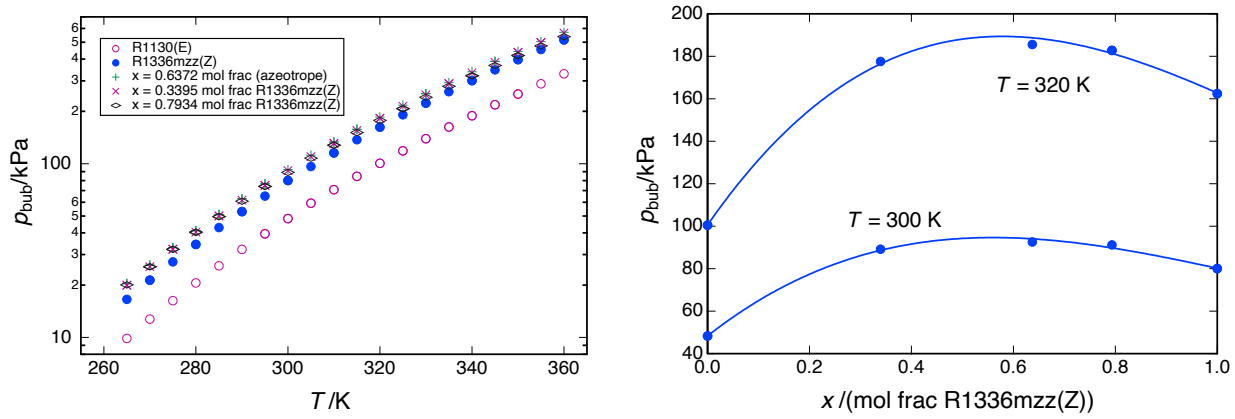

Fig. 3-2. Sample VLE results for the blend of R-1336mzz(Z) and R-1130(E).

3.2. (*p*, *ρ*, *T*, *x*) With Two-Sinker Densimeter

Two different density instruments were used in the current work. The first was a two-sinker densimeter with a magnetic suspension coupling. This type of instrument applies the Archimedes (buoyancy) principle to provide an absolute determination of the density. This general type of instrument is described by Wagner and Kleinrahm,[8] and our instrument is described in detail by McLinden and Lösch-Will.[9] Briefly, two sinkers of nearly the same mass

(~60 g) and same surface area (~41.5 cm^2), but very different volumes, were each weighed with a high-precision balance while they were immersed in the sample of unknown density. One sinker was made of tantalum (m = 60.094 633 g, V = 3.60 872 cm^3) and the other of titanium (m = 60.075 386 g, V = 13.315 284 cm^3). The basic form of the working equation for this type of instrument gives the fluid density ρ as:

$$\rho_{\text{fluid}} = \frac{(m_1 - m_2) - (W_1 - W_2)}{(V_1 - V_2)} \tag{3-2}$$

where m and V are the mass and volume of the sinkers, W are the balance readings, and the subscripts refer to the two sinkers. A magnetic suspension coupling transmitted the gravity and buoyancy forces on the sinkers to the balance, thus isolating the fluid sample from the balance. With the two-sinker method, systematic errors in the weighing and from other sources approximately cancel. Fig. 3-3 shows the entire instrument and Fig. 3-4 shows the two sinkers inside the cell.

Fig. 3-3. Two-sinker densimeter. The main part of the instrument is to the right of center with the vacuum thermostat below and balance above; the electronics are on the left side; a vacuum system for both evacuating the measuring cell and maintaining the vacuum thermostat is on the right. A separate system for calibrating sinker volumes sits to the right of the instrument rack.

In addition to the sinkers, two calibration masses (designated m_{cal} and m_{tare}) were also weighed by placing them directly on the balance pan. This provided a calibration of the balance and also the information needed to correct for magnetic effects as described by McLinden et al.[10] The four weighings (two sinkers and two calibration masses) yield a set of four equations that were

solved to yield a balance calibration factor α and a parameter ϕ characterizing the efficiency of the magnetic suspension coupling. With these additional terms, the fluid density is:

$$\rho_{\text{fluid}} = \left\{ \left[(m_1 - m_2) - \frac{(W_1 - W_2)}{\alpha\phi} \right] \Big/ (V_1 - V_2) \right\} - \rho_0 \tag{3-3}$$

where ρ_0 is the indicated density when the sinkers are weighed in vacuum. In other words, ρ_0 is an "apparatus zero." The density given by Eq. (3-3) compensates for the magnetic effects of both the apparatus and the fluid being measured. The difference of the value of ϕ from 1 indicates the magnitude of the force transmission error.[10]

The densimeter was thermostated by means of a multi-layer, vacuum-insulated thermostat. A copper shield with heaters at the top and side surrounded the measuring cell. An additional isothermal shield with heaters at the top and sides and a fluid cooling channel at the top surrounded the "inner shield"; it was maintained at a temperature approximately 1 K below the measuring-cell temperature. A chiller that circulated ethanol was used at temperatures below room temperature.

Fig. 3-4. Sinkers in the two-sinker densimeter (shown removed from the measuring cell). The titanium sinker is on the bottom, with the tantalum sinker above. The magnetic suspension coupling is at the top of the image; this comprises the electromagnet, which hangs from the balance; and the permanent magnet, which picks up the sinkers via "lifting forks;" the top of the measuring cell passes between the electromagnet and permanent magnet. In this photo, the titanium sinker is suspended off of its rest and is being weighed.

The temperature was measured with a 25 Ω standard platinum resistance thermometer (SPRT) and an AC resistance bridge referenced to a thermostated standard resistor. The temperature inside the measuring cell was constant within 5 mK. Pressures were measured with one of three vibrating-quartz-crystal type pressure transducers having full-scale pressure ranges of 2.8 MPa, 13.8 MPa, or 69 MPa. The transducers and pressure manifold were thermostated at T = 313.15 K to minimize the effects of variations in laboratory temperature.

A combination of measurements along isochores and along isotherms was carried out. The evacuated measuring cell was cooled and then the gas-phase sample from the sample bottle (see Sec. 3-5) was condensed into the measuring cell; higher pressures were obtained by closing the valve to the sample bottle and then increasing the cell temperature in steps along a pseudoisochore. Once a new setpoint temperature and pressure was reached an additional equilibration time of 30–60 minutes was allowed; four replicate density determinations were then carried out. When the maximum desired pressure along a pseudoisochore was reached, a portion of the sample was vented into a waste bottle to decrease the pressure; measurements were made in this manner along an isotherm to a minimum pressure of approximately 1 MPa or slightly above the bubble-point pressure, whichever was higher. Measurements then resumed at increasing temperatures along the next, lower-density pseudoisochore. This procedure did not require any pump and thus avoided any sample contamination that a pump might introduce.

Between each of the measured blend compositions and also before and after all of the testing, the densimeter cell was evacuated for a minimum of 36 h. This was done to clear the previously measured sample and to check the zero of the pressure transducers and the ρ_0 of the apparatus (Eq. 3-3). The ρ_0 varied by less than 0.0011 kg·m^{-3}.

The density in the vapor phase was measured along isotherms at temperatures up to 400 K. Each isotherm started at a low pressure (40 to 100 kPa); the pressure was increased in steps by cycling two pneumatic valves piped in series to introduce additional gaseous sample. With this technique the filling/pressure line was completely filled with vapor up to near the dew-point pressure, minimizing uncertainties in the composition. Each isotherm started with fresh sample.

The measurement uncertainty of the experimental density data measured with the two-sinker densimeter has been evaluated in previous works.[9] [11] [12] Only a brief description of the main uncertainty sources is given here. The main sources of the uncertainty in density, in order of significance, arose from the sinker volumes (V_1, V_2), the weighings of the sinkers and calibration masses (W_1, W_2, W_{cal}, W_{tare}) and their masses (m_1, m_2, m_{cal}, m_{tare}), and the apparatus zero ρ_0. The variance in the replicate balance readings was also included. The standard uncertainty in the density measurement is given by

$$u\left(\rho_{\text{fluid}}\right)/\text{kg}\cdot\text{m}^{-3} = \left[\left\{28\right\}^2 + \left\{0.2\left(T/K - 293\right)\right\}^2 + \left\{0.63p/\text{MPa}\right\}^2\right]^{1/2}\cdot 10^{-6}\,\rho/\text{kg}\cdot\text{m}^{-3} + 0.010 \tag{3-4}$$

where the term in brackets is from the uncertainty in the sinker volumes, and the final, constant term includes all other uncertainties.

The SPRT used to measure the temperature of the mixture was calibrated in our laboratory on ITS-90 from 83 K to 505 K by use of fixed-point cells. The standard uncertainty of the temperature, including the uncertainty in the fixed-point cells, drift in the SPRT and in the standard resistor, and any temperature gradients, is 3 mK. The pressure transducers were calibrated with one of two gas-operated piston gages. We estimated the standard uncertainty in pressure to be ($20\times10^{-6}\cdot p$ + 0.03 kPa) for the vapor-phase measurements and ($26\times10^{-6}\cdot p$ + 1.0 kPa) for the liquid-phase measurements. To the above uncertainty estimates we added the standard deviations actually observed in the multiple temperature, pressure, and balance readings made over the 12 minutes necessary to complete a single density determination.

For mixtures, a considerable fraction of the overall density uncertainty was due to uncertainty in the composition. This arose from the gravimetric preparation of the gas mixture used to charge the densimeter, and an additional contribution from possible adsorption of sample onto the inner walls of the sample cylinder, filling lines, measuring cell, etc. In other words, the composition in the measuring cell was not necessarily a simple ratio of the component masses loaded into the sample cylinder.

Fig. 3-5. shows examples of the measurements made with the two-sinker densimeter.

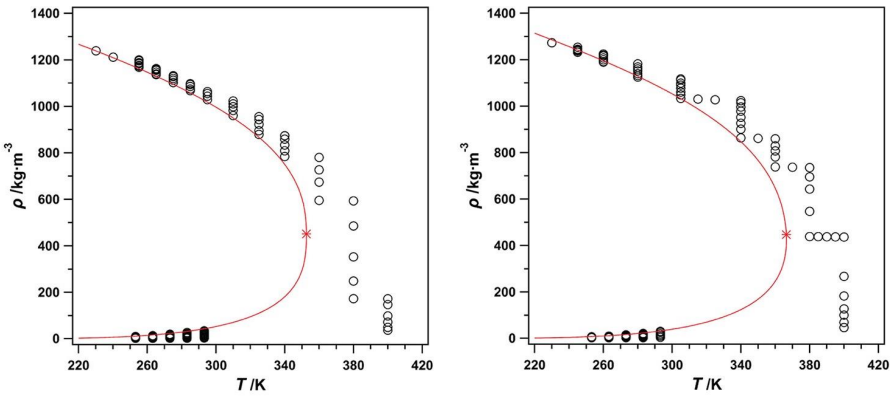

Fig. 3-5. Example density measurements made in the two-sinker densimeter; left panel is the R-32/1234yf blend at a composition of 0.6721 mol frac R-32; right panel is the blend R-32/1234ze(E) at a composition of 0.6667 mol frac R-32.

3.3. (p, ρ, T, x) With Vibrating-Tube Densimeter

A second density instrument—a vibrating-tube densimeter (VTD)—was utilized for the density measurements in Phase II of the project, namely R-1130(E) and the blends R-1132(E)/1234yf and R-1132(E)/32. This instrument has been described in detail elsewhere, [13] so only a brief description is provided here. At the heart of the apparatus is a commercial VTD, as shown in Fig. 3-6. Several modifications to the commercial instrument have been implemented, including the use of a custom-designed two-stage thermostat, which have improved overall temperature control as well as the accuracy of both temperature and pressure measurements. The instrument operates over temperatures from 270 K to 470 K and pressures up to 70 MPa.

Temperature was measured with a standard platinum resistance thermometer (SPRT), which was calibrated using a series of fixed-point cells and was controlled with thin-film heaters; a circulating bath was also used for temperatures ≤ 300 K. Once thermal equilibrium was achieved, the instrument temperature remained stable to within ± 5 mK. The combined standard uncertainty in temperature was ≤ 15 mK. Pressure was measured with an oscillating quartz crystal pressure transducer that was calibrated using a NIST-traceable piston gage and was controlled with a programmable syringe pump. The combined standard uncertainty in pressure is ≤ 5 kPa.

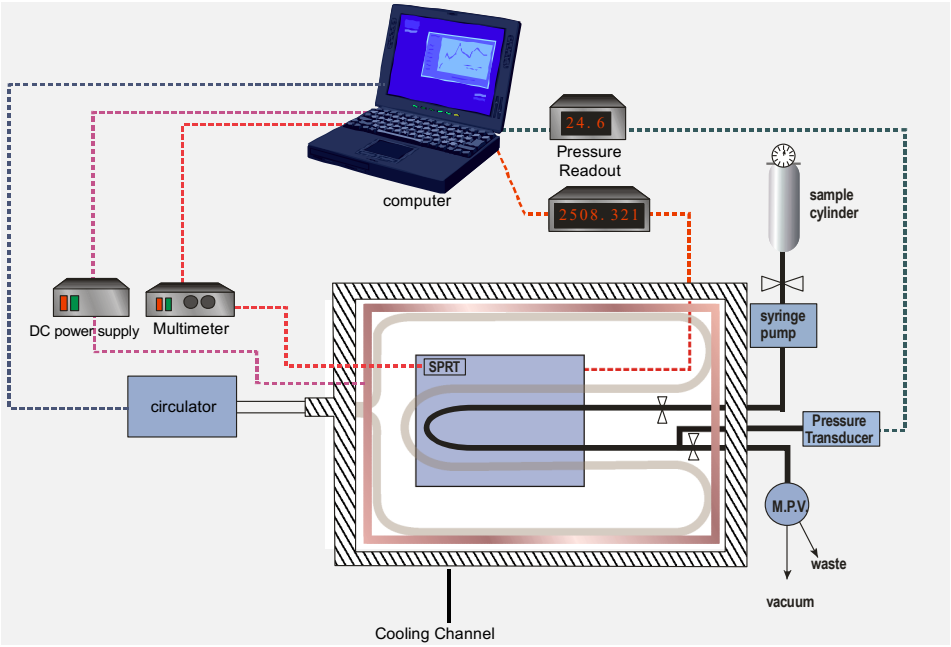

Fig. 3-6. Schematic of vibrating-tube densimeter.

The fundamental principle of this measurement technique is that the period of oscillation (τ) of a resonating hollow U-shaped tube can be related to the density (ρ) of the fluid that fills it. Mathematically, this can be expressed as

$$\rho_{\text{fluid}} = A\tau^2 - B \tag{3-5}$$

where A and B are apparatus-specific parameters that vary with both temperature and pressure and must be determined by calibration. Calibration involved first determining τ under vacuum (i.e., τ_0) over the full temperature range of the instrument. Next, the tube was filled with a fluid for which the density is well-known, and τ was measured over the full temperature and pressure range of interest. Ideally, the calibration fluid or fluids are chosen to cover the full range of expected densities for the sample fluid to be measured. In this work, we measured both toluene and R-1336mzz(Z) as potential calibration fluids but ultimately used just R-1336mzz(Z) for our instrument calibration. Although water is commonly used as a calibration fluid for VTDs, the density of water is significantly lower than those for the refrigerants studied

here and would thus be a poor calibration fluid for the measurement of high-density fluids. The density of R-1336mzz(Z), on the other hand, is very similar to that of R-1130(E).

The choice of calibration fluid is not the only important consideration; the choice of calibration equation is also important. A more detailed discussion of this issue can be found in Outcalt [14]. In this work, we have used the physically based model proposed by May et al. [15].

Prior to starting measurements, degassed liquid sample was loaded into the evacuated syringe pump and measurement cell. Once the VTD was filled with compressed liquid, measurements were made along isotherms starting from 270 K and increasing to 410 K in 20 K increments. For each isotherm, measurements were made from the highest to the lowest pressure, which in this work ranged from 30 MPa to 0.5 MPa. Measurement conditions were chosen to ensure that the sample remained in the compressed liquid phase throughout. Once measurements were completed for the full surface, additional measurements were made for at least two isotherms to check repeatability; poor repeatability could be an indication of sample decomposition. Repeat measurements were performed for selected mixture isotherms and for all of the isotherms for R-1130(E).

The R-1132(E)/32 and R-1132(E)/1234yf mixtures were in the gas phase, and this required a modified loading procedure. The syringe pump was disconnected from the apparatus and the sample bottle was connected directly to the sample inlet port. To load the samples, the instrument was cooled to approximately 260 K, and the sample bottle was heated for a minimum of 12 hours. The sample bottle was then opened to condense sample into the densimeter. After loading, measurements were made by raising the temperature of the densimeter in 2 K increments, thus making isochoric measurements of densities in the compressed-liquid phase.

The main sources of uncertainty for the density data collected with the VTD are the uncertainties associated with the temperature and pressure measurements and the uncertainty associated with the instrument calibration. Uncertainties associated with composition are typically negligible for a high-purity single-component fluid but may be significant if the sample is not of high purity or for a mixture if the composition is not well characterized. Therefore, the combined standard uncertainty in the reported densities, $u(\rho)$, can be expressed as

$$u(\rho_{\mathrm{fluid}}) = [u(T)^2 + u(p)^2 + u(\mathrm{cal})^2 + u(x)^2]^{1/2} \tag{3-6}$$

where the combined standard uncertainties for temperature ($u(T)$), pressure ($u(p)$), instrument calibration ($u(\mathrm{cal})$), and composition/purity ($u(x)$) are all in units of kg·m^{-3}. In this work, $u(T)$ included uncertainty contributions from the SPRT, the multimeter used to read the SPRT, the temperature calibration, temperature gradients, and temperature stability. Estimates for the individual contributions were combined using root sum of squares (RSS) to yield a value of 15 mK, which corresponds to a density uncertainty of 0.04 kg·m^{-3}. Similarly, $u(p)$ included contributions from the the transducer, the pressure calibration, the applied zero-pressure correction, and pressure stability. When combined using RSS, the resulting uncertainty was 5 kPa, which corresponds to a density uncertainty of 0.02 kg·m^{-3}. $u(\mathrm{cal})$ included contributions from the EOS for the calibration fluid (here we used R-1336mzz(Z)), the vacuum calibration, and

the fit to the calibration equation; when combined using RSS, $u(\mathrm{cal})$ was 0.2 kg·m^{-3}. Finally, $u(x)$ was approximately 0.17 kg·m^{-3}; this estimate was derived from sensitivity tests using REFPROP where (for the pure R-1130(E)) we varied the relative concentrations of the primary impurities identified during the compositional analysis or (for the mixtures) varied the composition by its estimated uncertainty.

The combined expanded uncertainty in density, $U(\rho)$, ranged from 0.05 % to 0.06 %. Fig. 3-7 shows example results.

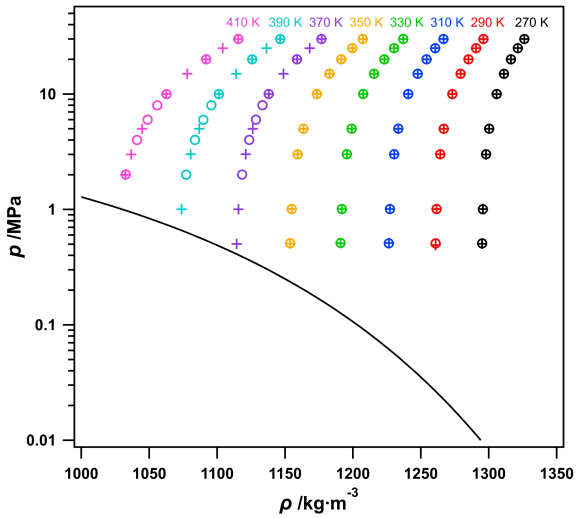

Fig. 3-7. Example measurements made with the vibrating-tube densimeter on R-1130(E); the symbols ○ and + represent data for the two sample loadings, and the line is the predicted saturation boundary.

3.4. Liquid-Phase Speed of Sound

The speed of sound was measured over wide ranges of temperature and pressure in a dual-path, pulse-echo-type instrument. In this technique, a piezoelectric transducer was located within a sample volume of the test fluid. It was excited with a sinusoidal burst, at the crystal resonance frequency, thus emitting ultrasonic pulses from each face of the crystal that traveled through the fluid sample, reflected off planar surfaces at each end of the sample volume, and returned to the transducer, which also served as the detector. The difference in the arrival times of the echo signals gives the speed of sound by

$$w = \frac{2\left(L_2 - L_1\right)}{\Delta t} \tag{3-7}$$

where w is the speed of sound, L_1 and L_2 are the path lengths, and Δt is the time difference. The differential nature of this technique cancels end effects and improves the accuracy.

A quartz crystal with a diameter of 24 mm, thickness of 0.36 mm, and resonant frequency of 8.000 MHz served as the ultrasonic transducer. The quartz crystal was “X-cut,” which means

that its thickness expands and contracts when a voltage is applied to electrodes on opposite faces of the crystal. It was excited with a 10-cycle sinusoidal burst from a function generator. The fluid path lengths on the opposite faces of the crystal were 30 mm and 12 mm (ratio of 2.5:1); these separations of the crystal and the reflectors were provided by tubular spacers fabricated of a machinable ceramic. A high-speed switch connected the crystal to the function generator during the input sinusoidal burst and then, after a delay of 6 μs, switched the crystal to the input of a three-stage amplifier (5× per stage for a total of 125×), which then fed into a digital storage oscilloscope. The echo signals were recorded for off-line analysis.

The measuring cell holding the crystal and fluid sample was contained in a pressure vessel rated to 93 MPa. This, in turn, was held in a thermostated liquid bath operating from –45 ˚C to 150 ˚C. A photo of the bath and associated fluid-handling manifold is shown as Fig. 3-8. A photo of the control electronics (which were located in the adjacent room) is shown as Fig. 3-9. A schematic of the measuring cell is shown as Fig. 3-10.

Fig. 3-8. Dual-path, pulse-echo, speed of sound instrument. Shown are the thermostat (left of center, which contains the measuring cell) and the fluid manifold and pressure transducer; a vacuum system for evacuating the measuring cell is to the left of the thermostat.

The temperature of the fluid bath was measured with a long-stem 25-ohm standard platinum resistance thermometer (SPRT); the temperature-sensing portion of the SPRT was located immediately adjacent to the pressure vessel, as indicated in Fig. 3-10. The resistance of the SPRT was ratioed to a standard resistor with an AC resistance bridge. The pressure was measured with a vibrating-quartz-crystal pressure transducer with a maximum pressure of 138 MPa. The transducer was held at room temperature.

The entire experiment was controlled by a PC running a custom control program. At each (T, p) state point, multiple echo signals were recorded and analyzed. The pressure of the fluid sample and the temperature of the thermostat bath were scanned every 30 s. The approach to equilibrium conditions was determined by monitoring three quantities: (1) the difference of the average temperature computed over the previous eight scans compared to the set-point

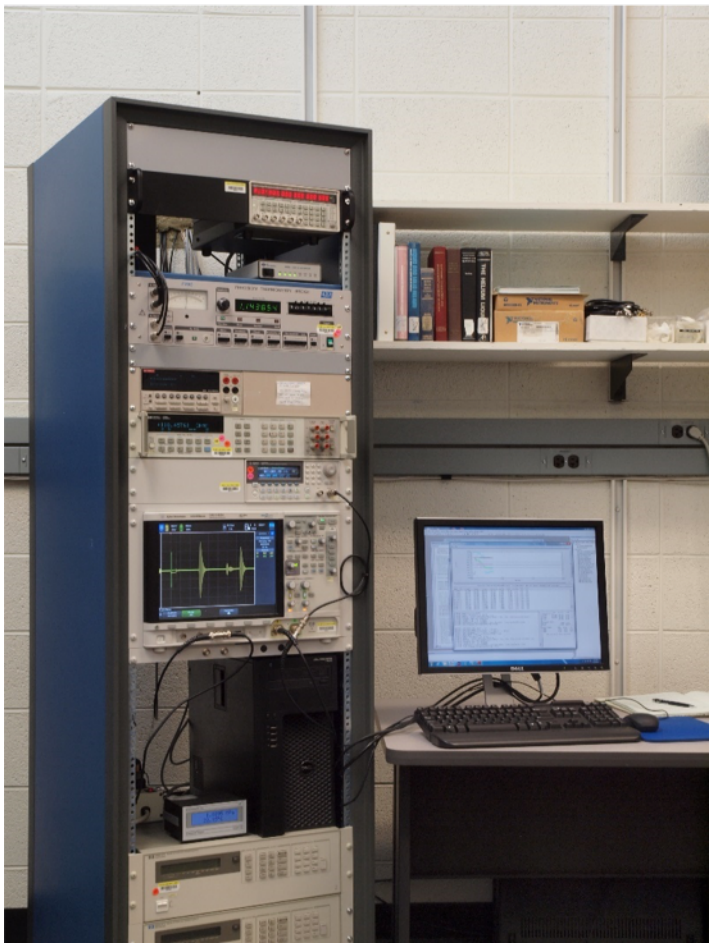

Fig. 3-9. Instrument rack for the pulse-echo speed of sound instrument.

temperature; (2) the standard deviation of the previous eight temperature scans; and (3) the rate of change of pressure with time, computed with a linear fit of the previous eight pressure readings. When all three of these were within preset tolerances a “converged” flag was set in the control program, and measurements commenced following an additional equilibration time of 20 minutes. A single measurement set comprised recording three echo signals and the four temperature and pressure readings made at the start and end of the set and between the recording of the echoes. Four such sets, spaced 10 minutes apart, were recorded before moving to the next (T, p) state point. These raw data were analyzed with a separate program to generate the (T, p, w) data points.

When measurements at the first temperature were completed, the temperature was increased by an increment of 5 K or 10 K; since the cell was completely filled with liquid, the increase in temperature also increased the pressure. Measurements continued along this pseudoisochore (line of nearly constant density) until either the desired maximum temperature or maximum pressure was reached. The bath was then cooled to the starting temperature of the next isochore, and a portion of the sample in the measuring cell was vented to a waste bottle to achieve a starting pressure for the next isochore of 1 MPa or the saturation pressure

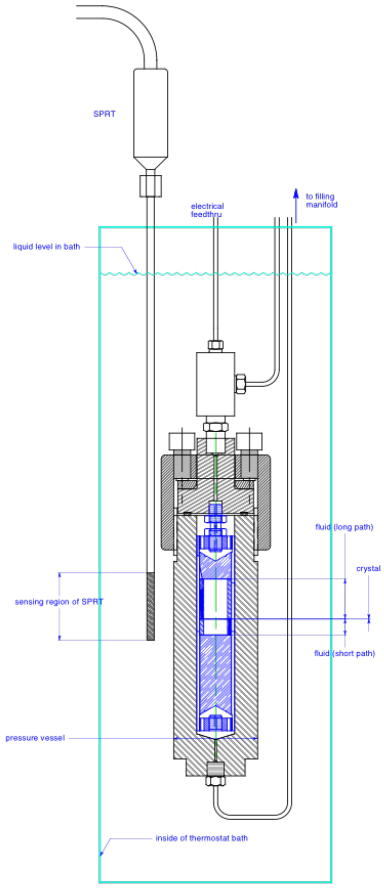

Fig. 3-10. Schematic diagram of the speed-of-sound measuring cell inside the pressure vessel and thermostatted bath.

(whichever was greater). The next isochore then commenced. This process was repeated to cover the liquid surface.

The difference of the path lengths in the measuring cell, i.e., $(L_2 - L_1)$ in Eq. 3-8, was calibrated as a function of temperature and pressure with measurements on propane over the temperature range of 260 K to 420 K, with pressures to 56 MPa. The propane speed of sound, as calculated with the equation of state (EOS) of Lemmon et al.[16], was taken as the known quantity in the calibration. The EOS, in turn, represents the high-accuracy propane measurements of Meier and Kabelac [17] with an average absolute deviation of 0.012 %. The RMS deviation of the calibration equation from the measurements was 0.010 %. Combining, in quadrature, the deviation of the EOS from the data of Meier and Kabelac [17] with the deviation of the path-length calibration equation from the present measurements yields an estimated combined standard uncertainty of 0.016 % arising from the calibration.

The SPRT, standard resistor, and resistance bridge were calibrated as a system over the range of 234.316 K to 429.749 K (–38.834 ˚C to 156.599 ˚C) with fixed-point cells (mercury triple point, water triple point, and indium freezing point). The standard uncertainty in the SPRT/resistor/bridge system was estimated as 3 mK. The short-term (minute-to-minute)

variations in the fluid-bath temperature were 2 mK or less. No long-term (hour-to-hour) variation was observed. The temperature gradients in the bath were less than 2.5 mK over the region of the pressure vessel. The combined standard (k = 1) uncertainty in the temperature measurement, including the effects of the SPRT, standard resistor, resistance bridge, calibration standards, stability of the fluid bath, and temperature gradients in the bath, was 4 mK.

The pressure transducer was calibrated by the manufacturer with piston gages; this calibration included a temperature-compensation term. The zero of the transducers was checked regularly (while the system was evacuated between samples) and readings were corrected for any drift in the zero. The standard uncertainty in pressure was 0.007 MPa.

When reporting the uncertainties in experimental data it is customary to combine the effects of the state-point uncertainty (i.e., the effects of the uncertainties in temperature, pressure, and composition) with those in the uncertainty of the primary measurand (i.e., the speed of sound):

$$U_c(w) = 2 \times 100 \times \left\{ u^2(w) + \left[\frac{\partial w}{\partial T}\right]^2 u^2(T) + \left[\frac{\partial w}{\partial p}\right]^2 u^2(p) \right\} \Big/ w \qquad (3\text{-}8)$$

where the $u(x)$ are the standard (k = 1) uncertainties in the different measurands (temperature, pressure, and speed of sound), the derivatives of the speed of sound with temperature and pressure are computed with an equation of state. The coverage factor of 2 corresponds to a 95 % confidence interval, and the factor of 100 converts the relative deviation to a percentage deviation. The $U_c(w)$ is the relative, combined, expanded (k = 2) uncertainty in the speed of sound; it averaged 0.07 % for the present measurements.

An example of the measurements carried out is depicted in Fig. 3-11.

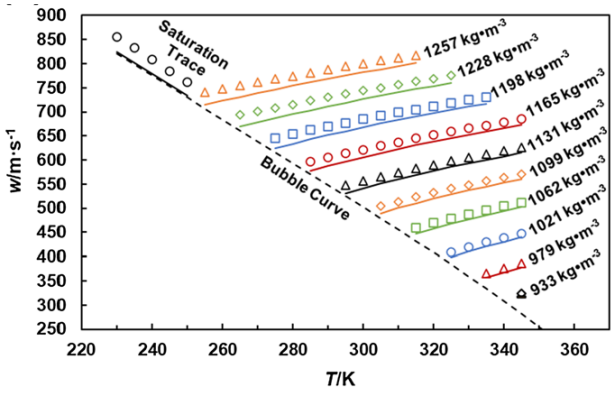

Fig. 3-11. Example speed-of-sound results showing the relationship between sound speed and temperature along isochores for the blend of R-32/1234ze(E) at a composition of 0.6667 mol frac R-32; the isochores extend to a maximum pressure of approximately 50 MPa or a temperature of 345 K. The “bubble curve” is the prediction from REFPROP, and the “saturation trace” are the points measured while the cell was liquid-filled, but the filling manifold was vapor-filled.

The speed-of-sound measurements on R-1132a presented an interesting challenge. The sound attenuation in the instrument was so strong with pure R-1132a that no usable signal could be obtained. The solution was to “dope” the R-1132a with a second component (here we used propane) that served to catalyze vibration–translation energy transfer in the fluid. In addition, up to 4096 echo signals were averaged to increase the signal-to-noise ratio. (For most other fluids, 256 echo signals were averaged.) Three R-1132a/propane blends were measured with propane compositions of 0.0274 to 0.0887 mol frac. The data at given values of composition and temperature were fitted to polynomials in pressure; these functions were used to interpolate speed of sound at even increments of temperature and pressure for each of the three compositions. The sound speeds at the three compositions for each isobar were then extrapolated to zero propane composition to obtain values for pure R-1132a. The resulting uncertainty in the speed of sound was 0.08 % to 0.11 %, which is larger than the usual uncertainty with this instrument, but which was still more than adequate for fitting an equation of state.

3.5. Mixture Preparation

All of the property measurements relied on preparation of the sample mixtures and accurate determination of their composition. The (p, ρ, T, x) and speed-of-sound measurements utilized gas-phase mixtures, while the VLE measurements utilized liquid-phase mixtures. The mixtures were prepared gravimetrically (by weighing) to achieve low uncertainties in the composition.

The pure-fluid refrigerants used to prepare the mixtures were used as received except that we degassed them (prior to preparing the mixtures) by freezing the pure components in liquid nitrogen, evacuating the vapor space, and thawing; this sequence was repeated until the residual pressure over the frozen sample was less than 0.01 Pa. We analyzed the pure-fluid refrigerants in-house using gas chromatography with either mass spectrometry (GC-MS) or NMR spectroscopy. Most of the samples we worked with were of very high purity (typically 99.9 % or better, as detailed in the individual journal papers), although the R-1130(E) sample had a purity of 99.7 %.

The gas-phase blends were prepared in aluminum gas cylinders of approximately 6, 10, or 13 L internal volume depending on the pressure of the blend. The sample mass was determined by a double substitution weighing design as described by Harris and Torres [18] with a nearly identical “tare” or reference cylinder serving as the main substitution mass. Further details are provided by Richter and McLinden.[19] The uncertainty of the measured gas-phase mixture compositions, arising from the weighings, was 0.0001 mole fraction. The sample cylinders were loaded to pressures corresponding to the dew-point pressure at T = 293.15 K. There may have been a small amount of liquid in the sample cylinders after filling, but they were heated continuously to T > 313 K for the duration of the testing to ensure that only single-phase vapor was present. Due to sorption effects, the composition of the sample in the measuring cell could be different from that calculated from the sample masses loaded into the sample cylinder, and this contributed an additional uncertainty of 0.0002 mole fraction. The combined, expanded uncertainty was estimated to be 0.00022 mole fraction.

The liquid-phase mixtures were prepared in 300 mL stainless steel cylinders. The fluid with the higher boiling point was added first, then the second component. The vapor space above the mixture samples was degassed by freezing the sample with liquid nitrogen and opening the cylinder to vacuum. After evacuation, the sample was then heated to drive volatile impurities (such as air) into the vapor space. The entire cycle (freezing, evacuation, and heating) was repeated a minimum of three times for each sample. Mixtures were prepared with the goal of filling the sample cylinder with about 280 mL of liquid at ambient temperature so that in each completed mixture cylinder there was a small vapor space above the liquid phase.

A balance with a precision of 0.1 mg was used in the preparation of the liquid-phase mixtures. Utilizing the double-substitution weighing design of Harris and Torres,[18] measurement of the mass of each component consisted of weighing four masses: (1) a reference cylinder of approximately the same mass and volume as the empty sample cylinder, (2) the sample cylinder, (3) the sample cylinder plus a 20 g sensitivity weight, and (4) the reference cylinder plus the 20 g sensitivity weight. This weighing sequence was repeated four times for each mass determination. The density of ambient air was calculated based on measurements of temperature, pressure, and relative humidity, and the weighings were corrected for the effects of air buoyancy. The standard deviation of the repeat weighings was at most 1.5 mg. The uncertainty in the composition due to the weighings was 0.0001 mole fraction or less. Because of the two-phase nature of the liquid-phase samples and because the weighings could determine only the overall (bulk) composition of the sample it was necessary to estimate the change in composition caused by the liquid/vapor fractionation inside the cylinder. This change was less than 0.0005 mole fraction, and its standard uncertainty was estimated to be less than 0.0001 mole fraction. Thus, the combined, expanded uncertainty in composition of the liquid-phase samples was estimated to be less than 0.00028 mole fraction.

The R-1132(E)/32 and R-1132(E)/1234yf mixtures were received pre-mixed from the manufacturer. These were supplied as two-phase mixtures and were expanded into larger gas cylinders to give a uniform vapor-phase composition. Their compositions were determined by NMR (nuclear magnetic resonance) spectroscopy, as detailed in the journal paper cited in Sec. 7.

4. Project Results—Property Modeling

Mixture properties are obtained by combining the properties of the constituent pure components with additional mixture terms. While equations of state (EOS) were available for most of the mixture components measured here, new EOS were developed for R-1130(E) and R-1132(E).

4.1. Data Survey

An early task in Phase I was to survey and assess the available literature data, thereby providing guidance for prioritizing the measurement efforts as well as providing data for the modeling efforts. We surveyed the existing literature data (as of early 2021) for refrigerant blends containing halogenated olefins (i.e., hydrofluoroolefins (HFOs), hydrochlorofluoroolefins (HCFOs), and hydrochloroolefins (HCOs)). Blends comprising a total of 36 pure fluids (12 olefins, 12 HFCs, 8 hydrocarbons, and 4 others) were considered. The data were primarily taken from the NIST SOURCE database; searches in the SciFinder database of the American Chemical Society and the Fridoc database of the International Institute of Refrigeration were also carried out. VLE data on 67 binary pairs were located; density data were located for 50 binary pairs; and there were 40 sources for all other data types. In total, more than 120 literature sources were identified and cataloged. (Note that some binary pairs were reported in multiple references, and some references reported multiple binary pairs and/or multiple data types.)

The results were presented in tabular and graphical forms to demonstrate the relative coverage of the data. The primary conclusion was that blends containing halogenated olefins remain only sparsely measured, and some classes of data (e.g., speed-of-sound data) are particularly sparse for blends containing halogenated olefins. The second part of this study compared the experimental data sets against the (then existing) thermodynamic models in NIST REFPROP and identified systems (of which there were many) for which additional measurements and refitting of the thermodynamic model were warranted.

4.2. Pure-Fluid Equation of State

The experimental thermodynamic properties of R-1130(E) and R-1132(E) were fitted to an equation of state explicit in the Helmholtz energy with density and temperature as independent variables. The form of the equation of state will reliably extrapolate outside the range of the experimental data, although with increased uncertainties.

4.2.1. Functional Form of the Equation of State

The equation of state is of the form:

$$a(\rho,T) = a^0(\rho,T) + a^r(\rho,T)\ , \tag{4-1}$$

where a is the Helmholtz energy, $a^0(\rho,T)$ represents the ideal-gas behavior and $a^r(\rho,T)$ accounts for the residual (or real-fluid) contribution. This form of equation is convenient since all the thermodynamic properties (including pressure, enthalpy, heat capacity, and speed of sound) can be obtained from derivatives of the Helmholtz energy.[20],[16] Eq. (4-1) is expressed in terms of the dimensionless Helmholtz energy $\alpha = a/(RT)$

$$\alpha(\delta,\tau) = \alpha^0(\delta,\tau) + \alpha^r(\delta,\tau)\,, \tag{4-2}$$

where $\delta = \rho/\rho_c$ and $\tau = T_c/T$ are the reduced density and inverse reduced temperature; T_c and ρ_c are the critical temperature and density, and the molar gas constant, R, is 8.314 462 618 J·mol^{-1}·K^{-1}.[21] There were limited data available for the critical parameters of the two fluids fitted here, and these were adjusted in the course of the EOS fitting.

The ideal-gas contribution of the Helmholtz energy in dimensionless form can be expressed as

$$\alpha^0 = \frac{h^0_{\rm ref}\tau}{RT_c} - \frac{s^0_{\rm ref}}{R} - 1 + \ln\frac{\delta\tau_{\rm ref}}{\delta_{\rm ref}\tau} - \frac{\tau}{R}\int_{\tau_{\rm ref}}^{\tau}\frac{c_p^0}{\tau^2}{\rm d}\tau + \frac{1}{R}\int_{\tau_{\rm ref}}^{\tau}\frac{c_p^0}{\tau}{\rm d}\tau\,, \tag{4-3}$$

where $\delta_{\rm ref} = \rho_{\rm ref}/\rho_c$, $\tau_{\rm ref} = T_c/T_{\rm ref}$, and $T_{\rm ref}$, $\rho_{\rm ref}$, $h_{\rm ref}^{\rm o}$, and $s_{\rm ref}^{\rm o}$ are used to define an arbitrary reference state. The ideal-gas heat capacity c_p^0 is given by

$$\frac{c_p^{\rm o}}{R} = n_0^{\rm o} + \sum_{i=1}^{3} n_i^{\rm o}\left(\frac{m_i^{\rm o}}{T}\right)^2 \frac{\exp(m_i^{\rm o}/T)}{[\exp(m_i^{\rm o}/T)-1]^2}, \tag{4-4}$$

and was fitted to values calculated from quantum statistical mechanics. The ideal-gas Helmholtz energy derived from Eqs. (4-3 and 4-4) may be written as

$$\alpha^{\rm o}(\tau,\delta) = \ln\delta + n_4^{\rm o} + n_5^{\rm o}\tau + (n_0^{\rm o}-1)\ln\tau + \sum_{i=1}^{3} n_{\rm i}^{\rm o}\ln\left[1-\exp\left(-\frac{m_{\rm i}^{\rm o}\tau}{T_{\rm c}}\right)\right] \tag{4-5}$$

where the n_4° and n_5° terms give values of h and s of 200 kJ/kg and 1.0 kJ/(kg K), respectively, for the saturated liquid at 0 °C. The values for n_i° and m_i° determined in this work are given in Tables 4-1 and 4-2 for R-1130(E) and R-1132(E), respectively.

The functional form of the residual contribution to the Helmholtz energy is

$$\begin{aligned}\alpha^{\rm r}(\tau,\delta) = &\sum_{i=1}^{K_1} n_i\tau^{t_i}\delta^{d_i} + \sum_{i=K_1+1}^{K_2} n_i\tau^{t_i}\delta^{d_i}\exp\left(-g_i\delta^{e_i}\right)\\ &+ \sum_{i=K_2+1}^{K_3} n_i\tau^{t_i}\delta^{d_i}\exp\left[-\eta_i\left(\delta-\varepsilon_i\right)^2 - \beta_i\left(\tau-\gamma_i\right)^2\right]\end{aligned} \tag{4-6}$$

The regression procedure utilized an in-house nonlinear least-squares algorithm developed by Lemmon and coworkers.[16, 22] We follow the procedure described in Ref.[16] and more recently summarized by Akasaka and Lemmon.[23, 24] The fitted coefficients and exponents are given in Table 4-1 for R-1130(E) and Table 4-2 for R-1132(E). Note that the two fluids fitted

here used a slightly different form of Eq. 4-6; the R-1130(E) did not use the $\exp[-\beta_i(\tau-\gamma_i)^2]$ terms, but this is accommodated by merely setting $\beta_i = 0$ in the third summation of Eq. 4-6.

4.2.2. Example for R-1130(E)

As an example of the performance of an equation of state developed in this work, the following figures illustrate the EOS for R-1130(E). Fig. 4-1 depicts the experimental data used in the fitting; included are vapor pressure, density, speed of sound, and heat capacity data both measured in the present work (which constitute the majority of the data) and from the literature.

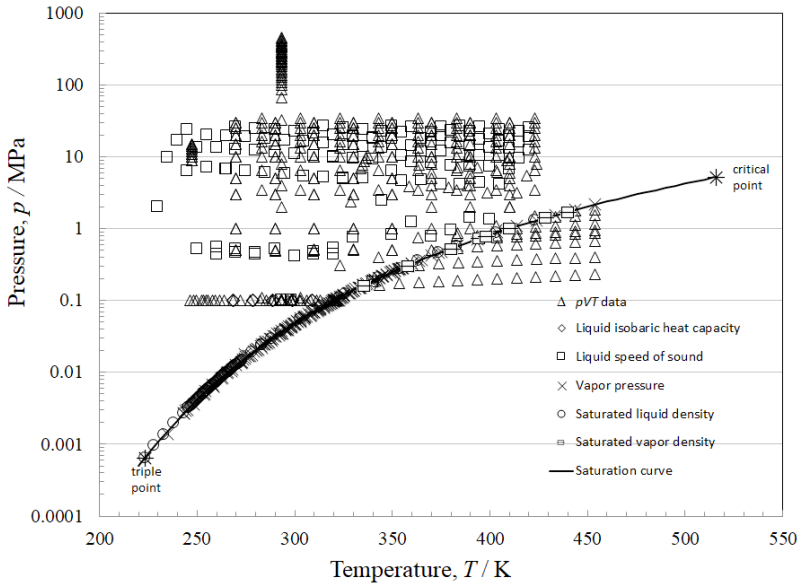

Fig. 4-1. Experimental data used in fitting the EOS for R-1130(E); shown are both data measured in the present work and literature data.

Examples of the deviations of the data from the final EOS are shown in Fig. 4-2. The left panel shows that the experimental densities are well represented by the EOS except at the highest temperature. The large deviations seen at T = 293 K are for measurements from a single source extending to pressures of 460 MPa; since the focus of this work is the modest pressures of refrigeration applications, these data were not used in the fit. The overall average absolute deviation is less than 0.3 % and the 136 data points of the present work, extending over a temperature range of 270 K to 410 K and pressures to 30 MPa, are fitted to 0.11 %. The right panel shows the deviations of the liquid-phase speed of sound. The present work makes up 145 of the 147 total data points and covers a temperature range of 230 K to 420 K with pressures to 27 MPa; the average absolute deviation is 0.10 %.

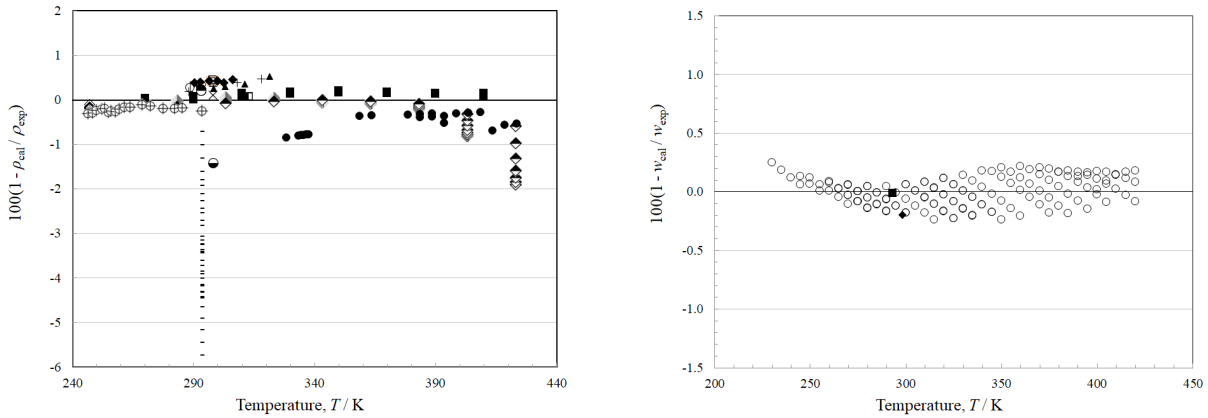

Fig. 4-2. Deviations of experimental data with the EOS for R-1130(E); the different symbols represent different sources. Left panel is liquid-phase density; the present work is shown as the solid black squares. Right panel is liquid-phase speed of sound; the present data are the open circles.

In addition to minimizing deviations of the EOS with experimental data it is important to examine the extrapolation behavior; this is especially important for a fluid such as R-1130(E) that does not have an extensive data set. As examples, the left panel of Fig. 4-3 depicts the speed of sound as a function of temperature from 0 K to 1000 K, drawn for isobars extending to pressures of 1000 MPa. This is an extreme extrapolation, and yet the EOS shows smooth behavior; only at temperatures below about 25 K is there an unphysical kink in the isobars, but this is well below the freezing point and of no practical consequence. The right panel of Fig. 4-3 shows the second, third, and fourth virial coefficients calculated by the EOS; again, they are smooth and show the general behavior predicted by theory; for example, *B*, *C*, and *D* all approach zero at high temperatures.

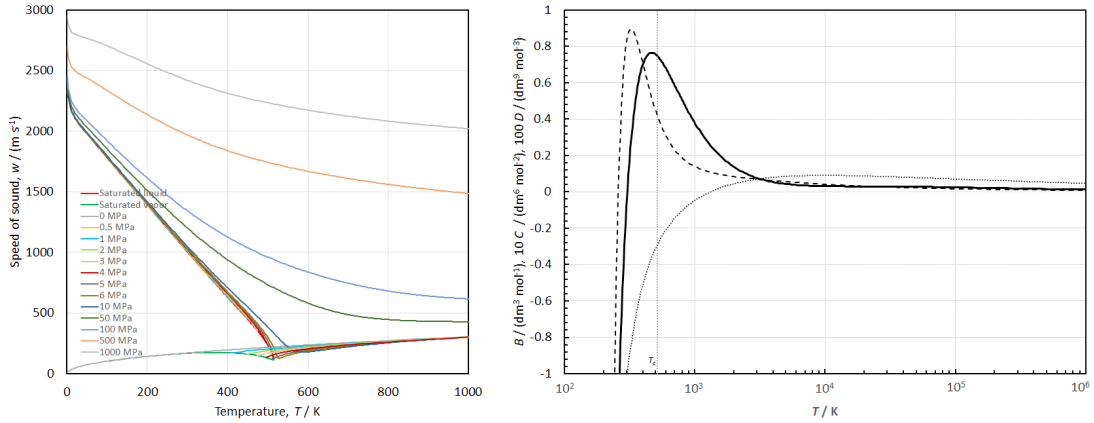

Fig. 4-3. Extrapolation behavior of the EOS for R-1130(E); left panel is speed of sound as a function of temperature with pressure to 1000 MPa; right panel is virial coefficients extending to $T = 10^6$ K; dotted curve, *B*; dashed curve, *C*; solid curve, *D*.

4.2.3. Equation of State Parameters

Table 4-1. Coefficients and exponents of the equation of state (Eqs. 4-5 and 4-6) for R-1130(E).

Critical parameters

T_c	ρ_c	p_c
515.69 K	4.54 mol·L^{-1}	5.25546 MPa

Parameters of the ideal-gas part of the equation of state (Eq. 4-5)

i	n_i	m_i
0	4	-
1	2.697	367.0
2	6.264	1246.0
3	3.041	4030.0
4	-14.91185845478433	-
5	8.646546650620836	-

Parameters to the residual part of the equation of state (Eq. 4-6); parameters not listed are not present for that value of *i.*

i	n_i	t_i	d_i	e_i	g_i	η_i	β_i	γ_i	ε_i
1	0.0256	1.	4						
2	0.9	0.188	1						
3	0.054	0.2496	2						
4	0.153	0.458	3						
5	-0.497874108699	0.77	1						
6	-0.990000049362	1.0385	2						
7	-0.318	0.9	1	1	2.43				
8	-0.973	1.21	1	2	1.236548				
9	-0.098	4.7	1	3	0.722				
10	-0.034	6.61575	2	3	1.483				
11	-0.0971	2.257	3	3	0.2255				
12	-0.26	3.2664	1			5.10245	0	1	-0.31662
13	-0.135	3.59	2			4.572	0	1	0.065
14	-0.21	1.2	1			4.63	0	1	-0.28568
15	-0.197	1.42	1			1.785	0	1	0.99

Table 4-2. Coefficients and exponents of the equation of state (Eqs. 4-5 and 4-6) for R-1132(E).

Critical parameters

T_c	ρ_c	p_c
348.82 K	6.793 mol·L^{-1}	5.1737 MPa

Parameters of the ideal-gas part of the equation of state (Eq. 4-5), note: the term i = 3 is not present for R-1132(E)

i	n_i	m_i
0	4	-
1	4.896	730.0
2	7.111	2259.0
3	-	-
4	-8.59622227406093	-
5	6.44053327169375	-

Parameters to the residual part of the equation of state (Eq. 4-6); parameters not listed are not present for that value of i.

i	n_i	t_i	d_i	e_i	g_i	η_i	β_i	γ_i	ε_i
1	0.033144696	1.	4						
2	1.8996205	0.32	1						
3	-2.190517288130	0.71	1						
4	-0.8165909562367	1.2	2						
5	0.22857476	0.7	3						
6	-1.650708	2.09	1	2	1				
7	-1.4409077	2.24	3	2	1				
8	0.60536471	1.17	2	1	1				
9	-0.66134087	2.2	2	2	1				
10	-0.016787895	0.823	7	1	1				
11	0.31476822	3.14	1			34.4	1017.	1.0617	0.9637
12	-0.31991607	4.	1			34.28	1009.	1.062	0.9636
13	2.2172762	1.25	1			1.303	1.011	1.327	0.8535
14	-0.42786753	1.476	1			1.855	1.05	1.05	1.15
15	-0.41335541	1.5	1			1.29	1.33	1.157	1.302
16	0.13023087	0.73	1			1.17	1.61	1.183	1.54
17	-0.30592804	1.535	1			2.165	0.8	1.2	0.786

4.3. Mixture Modeling

The multi-fluid modeling used in NIST REFPROP yields the most accurate mixture models available today. This approach combines the most-accurate pure fluid equations of state with reducing and departure functions to correct for the changes in the thermodynamic properties caused by mixture interactions The refrigeration industry has been using this multi-fluid modeling approach for many years. In this framework, the equations of state for the pure components are given in terms of the reduced Helmholtz energy, i.e., $\alpha = a/(RT)$, as outlined in the previous section.

4.3.1. Mixture equation of state

The same thermodynamic identities hold for mixtures as for pure fluids. The Helmholtz energy for a mixture is commonly obtained as the sum of terms from the pure fluids with a departure term:

$$\alpha^{\mathrm{r}} = \sum_{i=1}^{N} x_i \alpha_{0,i}^{\mathrm{r}}(\tau,\delta) + \sum_{i=1}^{N}\sum_{j=i+1}^{N} F_{ij} x_i x_j \alpha_{ij}^{\mathrm{r}}(\tau,\delta) \tag{4-7}$$

where the first summation arises from a composition-weighted sum of the pure fluid EOS terms and the double summation is the departure term, with the α_{ij}^{r} given by

$$\alpha_{ij}^{\mathrm{r}} = \sum_k n_k \tau^{t_k} \delta^{d_k} \exp\left[-\mathrm{sgn}(l_k)\delta^{l_k}\right] \tag{4-8}$$

where the sgn function is the sign of the value: zero for an argument of zero, and 1 for positive arguments. This departure function provides additional flexibility, but it is used only when needed to fit non-ideal behavior and only when there are sufficient data on a binary pair so that the model is not statistically over-fit.

For mixtures the key feature is that the pure-fluid EOS in Eq. 4-7 are not evaluated at the temperature and density of the mixture, but rather at a reduced temperature and density given by $\tau = T_{\mathrm{r}}(\bar{x})/T$ and $\delta = \rho/\rho_{\mathrm{r}}(\bar{x})$. The reducing functions are given by

$$T_{\mathrm{r}}(\bar{x}) = \sum_{i=1}^{N}\sum_{j=1}^{N} x_i x_j \beta_{T,ij}\gamma_{T,ij} \frac{x_i + x_j}{\beta_{T,ij}^2\left(x_i + x_j\right)} \left(T_{c,i}\cdot T_{c,j}\right)^{0.5} \tag{4-9}$$

$$\frac{1}{\rho_{\mathrm{r}}(\bar{x})} = \sum_{i=1}^{N}\sum_{j=1}^{N} x_i x_j \beta_{V,ij}\gamma_{V,ij} \frac{x_i + x_j}{\beta_{V,ij}^2\left(x_i + x_j\right)} \times \frac{1}{8}\left(\frac{1}{\rho_{c,i}^{1/3}} + \frac{1}{\rho_{c,j}^{1/3}}\right)^3 \tag{4-10}$$

Thus, the reducing functions have four adjustable parameters per *ij* pair plus possibly additional parameters associated with the departure function. (In cases where very limited data are available, only the γ_T parameter is fit; here only for the R-1132a/1234yf blend were just β_T and γ_T fitted because only VLE data were measured, but otherwise all the parameters were fitted.)

Mixtures with three or more components are modeled in terms of the constituent binary pairs. For example, a blend of components A, B, and C would be modeled in terms of the A/B, A/C, and B/C binary pairs. Thus, the present measurements were carried out on binary mixtures, even though ternary (three-component) or higher mixtures are also of interest.

4.3.2. Parameter Optimization

We used the parameter optimization approach described in [25]. The parameters $\beta_{T,ij}$ and $\gamma_{T,ij}$ were obtained for each binary pair individually, leaving the other interaction parameters set to their default values. The experimental data were added to the database of experimental data used in the fitting tool. Then a python script was launched which carried out the optimization, doing a stochastic global optimization over the two interaction parameters with the DEAP software package. The approach used was a classical evolutionary optimization methodology with crossover, mutation, etc. The mixture behavior for the blends studied here is ideal enough that simpler optimization approaches could have been used, but this implementation has proven to be reliable for fitting interaction parameters, particularly for fitting interaction parameters to outputs of iterative routines that can fail for a variety of different reasons. Failures of iterative routines are handled by adding a large contribution to the cost function. Derivatives are not used in the optimization approach, so the cost function to be minimized need not be differentiable. The parameters thus obtained are given in Tables 4-3 and 4-4. Note that "interim models" were previously published by Bell [26] for R-125/1234yf, R-1234ze(E)/227ea, and R-1234yf/152a; the parameters here supplant the earlier ones.

Table 4-3. Mixing parameters (Eq. 4-9 and 4-10) for the binary pairs investigated in this work; an F_{ij} = 0 for a binary pair indicates that no departure function applies for that pair.

Binary pair	$\beta_{T,ij}$	$\gamma_{T,ij}$	$\beta_{v,ij}$	$\gamma_{v,ij}$	F_{ij}
R-32/1234yf	1.0110	0.9670	1.0079	1.0377	1.0
R-32/1234ze(E)	1.0051	0.9461	0.9990	1.0298	1.0
R-1234ze(E)/227ea	1.0012	0.9892	0.9993	1.0016	1.0
R-1234yf/152a	0.9960	0.9781	0.9997	1.0086	1.0
R-125/1234yf	1.0000	0.9980	0.9982	1.0061	1.0
R-1132a/1234yf	0.9921	1.0169	1.0000	1.0000	0.0
R-1336mzz(Z)/1130(E)	0.9740	0.9195	1.1480	0.9251	1.0
R-1132(E)/32	0.9509	1.0281	1.0336	1.0040	0.0
R-1132(E)/1234yf	0.9835	0.9999	0.9972	1.0197	0.0

Table 4-4. Departure functions (Eq. 4-8) for the binary pairs investigated in this work; note that not all of the binary pairs have a departure function.

Binary pair	k	n_k	t_k	d_k	l_k
R-32/1234yf	0	0.449487	2.538296	1	1
	1	-0.099708	3.208604	2	1
	2	0.098897	0.456509	3	1
R-32/1234ze(E)	0	0.295192	0.500457	1	1
	1	-0.737904	3.104735	2	1
	2	0.542962	3.201720	3	1
	3	-0.201951	2.567118	4	1
R-1234ze(E)/227ea	0	-0.057178	1.290298	1	1
	1	0.031318	0.038796	2	1
	2	-0.027496	2.640532	3	1
R-1234yf/152a	0	0.009165	3.221227	1	1
	1	0.014392	1.007082	2	1
	2	-0.014246	3.790953	3	1
R-125/1234yf	0	-0.032013	0.008030	1	1
R-1336mzz(Z)/1130(E)	0	-0.277036	2.956973	1	1

5. Significant Accomplishments and Conclusions

This project has provided data and models that will allow industry to assess new refrigerants and refrigerant blends. The thesis behind this project was that the measurement and modeling of basic thermodynamic data come at a modest cost but would enable the evaluation of new fluids and blends. The usual sequence for qualifying a new refrigerant is to first consider the toxicity and manufacturability and then test in equipment; but these are lengthy and expensive processes that also require significant quantities of refrigerant (up to hundreds of kilograms). In contrast, thermodynamic measurements take a few months and require a few hundred grams of sample. If cycle and equipment simulations, which are enabled by the thermodynamic models, fail to show promising performance, those expensive steps can be bypassed altogether, and effort can be redirected to other fluids.

Speed-of-sound measurements on pure R-1132a were not possible due to strong sound absorption. We pivoted to measuring three blends of R-1132a mixed with small amounts of propane and extrapolated these mixture data to zero propane concentration to obtain the required sound speed values for pure R-1132a.

The measurements with R-1132(E) presented a challenge in that the pure fluid was revealed (by the manufacturer) to be unstable over certain ranges of temperature and pressure, as detailed by Goto et al.[27] Work with such a fluid would likely not satisfy the NIST safety review (or would require costly and time-consuming modifications to testing protocols). This knowledge was received after the initial work plan based on measuring the pure fluid was established. We pivoted to measuring blends with R-1234yf or R-32, which were prepared by the manufacturer. The blends suppressed the instability of the R-1132(E), and measurements could proceed.

Links to archival journal papers generated by this project are given in Sec. 7. These provide full details of the work, including experimentally measured data and numerical parameters for the resulting property models.

The intent of the project was to provide data and models to industry, with industry taking on the task of evaluating whether the investigated blends were promising for their own products. The refrigerants and blends that were investigated were decided by an industry working group convened by the Air-Conditioning, Heating and Refrigeration Technology Institute (AHRTI), ensuring that they would be relevant to industry interests.

6. Path Forward

This project generated data and models that were enabling, in the sense that they *enabled* the evaluation of different refrigerants in equipment. These were transferred to industry via published papers, and data files compatible with the NIST REFPROP database are available at the link presented in the Supplemental Information section at the end of this report. Any commercialization of the refrigerants and blends considered here is the purview of industry. As such, this work represents an end state.

But with that said, the refrigeration industry continues to face uncertainty around future refrigerants. A particular concern is possible regulations around PFAS or per- and polyfluoroalkyl substances. PFAS (often referred to as “forever chemicals”) have a high persistence in the environment, and some members of this chemical class are toxic. Because of this, PFAS have come under increased regulatory scrutiny. A proposed European Union (EU) regulation would restrict the use of the entire chemical class of PFAS [28]. This regulation would affect the availability of the many refrigerants that are included in the EU definition of PFAS, namely a “substance that contains at least one fully fluorinated methyl ($–CF_3$) or methylene ($–CF_2–$) carbon atom (without any H/Cl/Br/I attached to it)”. The U.S. EPA has proposed the regulation of six specific PFAS chemicals in drinking water [29]; none of these are refrigerants. Nevertheless, the multinational nature of the refrigeration industry means that U.S. manufacturers would have to meet any regional regulations to sell in those markets.

A related issue is the atmospheric breakdown products of refrigerants. For some fluids that contain a $–CF_3$ group in the molecule, the breakdown products can include trifluoracetic acid or TFA ($CF_3C=OOH$), which is persistent in the environment.[30] The formation, fate, and potential effects of TFA have been studied for many years and continues to be a subject of debate. Furthermore, TFA itself falls under some definitions of PFAS. As with PFAS, U.S. industry may need to accommodate TFA regulations in other parts of the world.

The concerns around TFA and PFAS would make it prudent to consider what additional property data would be required to implement refrigerants and blends that are not PFAS or TFA-generating. These center around R-32, R-152a, R-1132(E), and R-1132a as well as the so-called natural refrigerants CO_2, ammonia, and hydrocarbons. Here, the equation of state for R-152a is old and should be refit, and the EOS for R-1132a has known deficiencies. The current project has addressed R-1132(E). A new EOS for R-32 is in progress in Japan. The current EOS for CO_2, ammonia, and the hydrocarbons are generally very good. The greatest need for additional data and modeling is for mixtures. CO_2-containing blends often display non-ideal behavior, such that they cannot be reliably predicted in the absence of data. The current project has started to address the data needs for blends containing R-1132a or R-1132(E). There are generally good data available for hydrocarbon blends, but many blends are based on a generalized model, which could be improved. Blends of hydrocarbons with HFCs or HFOs are generally sparse, and additional data would be required if such blends were commercialized.

An August 2024 survey of members of the AHRTI-convened industry working group were largely in line with the above. In addition, they expressed interest in 3,3,3-trifluoropropyne and R-1132(Z).

7. Products—Published Papers

The results from this project have been published in archival journals, and these papers contain the full details of the work. For reasons of space, links to these papers are provided below in lieu of reproducing the entire papers (which would run to more than 500 pages). In all cases a link to the published version is provided. These links may be to the paper's page on the publisher's website, rather than to the paper itself; click on "Download PDF" or "View PDF" to access the paper. In cases where the paper is not open access and a reader may not have subscription access to a particular journal, a second link is provided either to the PubMed repository or to a NIST site providing a version described as the "final accepted manuscript." The properties-related publications from the parallel SERDP-funded project are also listed.

Phase I Publications:

Bell, I. H.; Riccardi, D.; Bazyleva, A.; McLinden, M. O., Survey of data and models for refrigerant mixtures containing halogenated olefins. *J. Chem. Eng. Data* **2021,** *66*, 2335-2354. https://pubs.acs.org/doi/pdf/10.1021/acs.jced.1c00192 (open access).

Rowane, A.; Perkins, R. A., Speed of sound measurements of binary mixtures of difluoromethane (R-32) with 2,3,3,3-tetrafluoropropene (R-1234yf) or *trans*-1,3,3,3-tetrafluoropropene (R-1234ze(E)) refrigerants. *Int. J. Thermophysics* **2022,** *43*, 46. https://doi.org/10.1007/s10765-021-02966-y (publisher's website), https://pmc.ncbi.nlm.nih.gov/articles/PMC10091396/ (manuscript version).

Outcalt, S. L.; Rowane, A., Bubble point measurements of three binary mixtures of refrigerants: R-32/1234yf, R-32/1234ze(E) and R-1132a/1234yf. *J. Chem. Eng. Data* **2022,** *67*, 932–940. https://pubs.acs.org/doi/pdf/10.1021/acs.jced.1c00871 (publisher's website), https://pmc.ncbi.nlm.nih.gov/articles/PMC10020978/ (manuscript version).

Rowane, A. J.; Perkins, R. A., Speed of sound measurements of binary mixtures of hydrofluorocarbons [pentafluoroethane (R-125), 1,1-difluoroethane (R-152a), or 1,1,1,2,3,3,3-heptafluoropropane (R-227ea)] with hydrofluoroolefins [2,3,3,3-tetrafluoropropene (R-1234yf) or *trans*-1,3,3,3-tetrafluoropropene (R-1234ze(E))]. *Int. J. Thermophys.* **2022,** *43*, 127. https://doi.org/10.1007/s10765-022-03052-7 (publisher's website), https://pubmed.ncbi.nlm.nih.gov/39381076/ (manuscript version).

Fortin, T. J.; McLinden, M. O., Vapor and liquid (p-ρ-T-x) measurements of binary refrigerant blends containing R-32, R-152a, R-227ea, R-1234yf, and R-1234ze(E). *J. Chem. Eng. Data* **2023**, *68*, 1565–1583. https://doi.org/10.1021/acs.jced.3c00104 (publisher's website), https://pmc.ncbi.nlm.nih.gov/articles/PMC11497627/ (manuscript version).

Bell, I. H., Mixture model for refrigerant pairs R-32/1234yf, R-32/1234ze(E), R-1234ze(E)/227ea, R1234yf/152a, and R-125/1234yf. *J. Phys. Chem. Ref. Data* **2023** *52***,** 013101. https://doi.org/10.1063/5.0135368 (publisher's website), https://tsapps.nist.gov/publication/get_pdf.cfm?pub_id=935321 (manuscript version)

Rowane, A. J.; Perkins, R. A., Speed of sound measurements of binary mixtures of 1,1-difluoroethylene (R-1132a) + propane and derived speed of sound of pure R-1132a, *Int. J. Thermophys.* **2024,** *45*, 148. https://doi.org/10.1007/s10765-024-03431-2 (open access).

Phase II Publications:

Rowane, A. J., Speed of sound measurements of R-1130(E) and an azeotropic blend of R-1336mzz(Z)/1130(E). *Int. J. Thermophys.* **2024,** *45*, 142. https://doi.org/10.1007/s10765-024-03416-1 (open access).

Rowane, A. J.; Outcalt, S. L., Bubble point measurements of *cis*-1,1,1,4,4,4-hexafluorobutene [R-1336mzz(Z)] + *trans*-1,2-dichloroethene [R-1130(E)] mixtures. *Int. J. Thermophys.* **2024,** *45*, 96. https://doi.org/10.1007/s10765-024-03388-2 (open access).

Fortin, T.J., Outcalt, S.L., Compressed liquid (*p-ρ-T*) measurements of *trans*-1,2-Dichloroethene [R1130(E)], Int. J. Thermophys. **2025**, *46, 74*. https://doi.org/10.1007/s10765-025-03526-4 (open access).

Rowane, A.J., Rasmussen, E.G., Speed of sound measurements of binary mixtures of *trans*-1,2-difluoroethylene (R-1132(E)) with difluoromethane (R-32) or 2,3,3,3-Tetrafluoropropene (R-1234yf), *J. Chem. Eng. Data* **2025**, *70*, 817-826. https://pubs.acs.org/doi/pdf/10.1021/acs.jced.4c00531 (publisher's website), https://tsapps.nist.gov/publication/get_pdf.cfm?pub_id=958769 (manuscript version)

Huber, M.L., Kazakov, A.F., Lemmon, E.W., Equation of state for the thermodynamic properties of *trans*-1,2-dichloroethene [R-1130(E)], *Int. J. Thermophys.* **2025**, *46,* 76. https://doi.org/10.1007/s10765-025-03535-3 (open access).

Publications containing property data and modeling from the parallel SERDP-funded project:

Domanski, P.; McLinden, M.; Babushok, V.; Bell, I.; Fortin, T.; Hegetschweiler, M.; Huber, M.; Kedzierski, M.; Kim, D.; Lin, L.; Linteris, G.; Outcalt, S.; Payne, W.; Perkins, R.; Rowane, A.; Skye, H. *Low-GWP Non-Flammable Alternative Refrigerant Blends for HFC-134a: Final Report, NIST Interagency/Internal Report (NISTIR) 8455*; National Institute of Standards and Technology, Gaithersburg, MD: **2023**. https://doi.org/10.6028/NIST.IR.8455 (final report of entire project, open access)

Outcalt, S. L.; Rowane, A. J., Bubble point measurements of mixtures of HFO and HFC refrigerants. *J. Chem. Eng. Data* **2021**, *66*, 4670-4683. https://pubs.acs.org/doi/pdf/10.1021/acs.jced.1c00654 (publisher's website), https://pubmed.ncbi.nlm.nih.gov/36937169/ (manuscript version).

Bell, I., H., Mixture models for refrigerants R-1234yf/134a, R-1234yf/1234ze(E), and R-134a/1234ze(E) and interim models for R-125/1234yf, R-1234ze(E)/227ea, and R-1234yf/152a. *J. Phys. Chem. Ref. Data* **2022**, *51*, 013103. https://doi.org/10.1063/5.0086060 (publisher's website), https://tsapps.nist.gov/publication/get_pdf.cfm?pub_id=933859, (manuscript version).

Rowane, A. J.; Bell, I. H.; Huber, M. L.; Perkins, R. A., Thermal conductivity of binary mixtures of 1,1,1,2-tetrafluorethane, 2,3,3,3-tetrafluoropropene, and *trans*-1,3,3,3-tetrafluoropropene refrigerants. *Ind. Eng. Chem. Res.* **2022**, *66*, 1365-1377. https://pubs.acs.org/doi/pdf/10.1021/acs.iecr.2c01924 (publisher's website), https://pmc.ncbi.nlm.nih.gov/articles/PMC10092145/ (manuscript version).

Rowane, A. J.; Perkins, R. A., Speed of sound measurements of binary mixture of 1,1,1,2-tetrafluoroethane (R-134a), 2,3,3,3-tetrafluoropropene (R-1234yf), and 1,3,3,3-tetrafluoropropene (R-1234ze(E)) refrigerants. *J. Chem. Eng. Data* **2022**, *67*, 1365-1377. https://pubs.acs.org/doi/pdf/10.1021/acs.jced.2c00037 (publisher's website), https://pmc.ncbi.nlm.nih.gov/articles/PMC10092117/ (manuscript version)

Fortin, T. J.; McLinden, M. O., Vapor and liquid (p-ρ-T-x) measurements of binary refrigerant blends containing R-134a, R-1234yf, and R-1234ze(E). *J. Chem. Eng. Data* **2023,** *68*, 1543–1564. https://pubs.acs.org/doi/pdf/10.1021/acs.jced.3c00103 (publisher's website), https://pmc.ncbi.nlm.nih.gov/articles/PMC11465363/ (manuscript version).

8. Project Team and Roles

Mark O. McLinden: principal investigator; conceptualization; project administration; supervision; investigation (density measurements); writing—original draft

Katrina N. Avery: investigation (assist with density measurements using vibrating-tube densimeter)

Ala Bazyleva: data curation (survey of literature data)

Ian H. Bell: data curation (survey of literature data); analysis and investigation (lead for mixture property modeling)

Tara J. Fortin: investigation (lead for density measurements)

Marcia L. Huber: analysis and investigation (pure-fluid EOS modeling)

Andrei F. Kazakov: analysis and investigation (quantum mechanical modeling of ideal-gas properties)

Eric W. Lemmon: analysis and investigation (pure-fluid EOS modeling)

Stephanie L. Outcalt: investigation (lead for VLE measurements)

Richard A. Perkins: investigation (speed of sound measurements)

Elizabeth G. Rasmussen: investigation (assist with speed of sound measurements)

Demian Riccardi: data curation (survey of literature data)

Aaron J. Rowane: investigation (lead for speed of sound measurements, assist with VLE measurements, assist with mixture property modeling)

References

1. U.S. Energy Information Administration. *Annual Energy Outlook 2023*. 2023; Available from: https://www.eia.gov/outlooks/aeo/data/browser/.
2. United Nations Environment Programme, *Decision XXVIII/--- Further Amendment of the Montreal Protocol*, in *Twenty-Eighth Meeting of the Parties to the Montreal Protocol on Substances that Deplete the Ozone Layer, Kigali, 10–14 October 2016*. 2016: downloaded 19 October 2016 from: http://unep.org/newscentre/Default.aspx?DocumentID=27086&ArticleID=36283&l=en.
3. U.S. Environmental Protection Agency. *Background on HFCs and the AIM Act*. 2020; Available from: https://www.epa.gov/climate-hfcs-reduction/background-hfcs-and-aim-act.
4. Lemmon, E.W., et al., *NIST Standard Reference Database 23: Reference Fluid Thermodynamic and Transport Properties—REFPROP, Version 10.0*. 2018, National Institute of Standards and Technology, Gaithersburg, MD.
5. Domanski, P., et al., *Low-GWP Non-Flammable Alternative Refrigerant Blends for HFC-134a: Final Report, NIST Interagency/Internal Report (NISTIR) 8455*. 2023, National Institute of Standards and Technology, Gaithersburg, MD.
6. Outcalt, S.L. and E.W. Lemmon, *Bubble point measurements of eight binary mixtures for organic rankine cycle applications.* J. Chem. Eng. Data, 2013. **58**: p. 1853-1860.
7. Hust, J.G., J. Filla, and D.R. Smith, *A modified digital PID temperature controller for thermal property measurements.* Journal of Thermal Insulation, 1987. **11**(10): p. 102-107.
8. Wagner, W. and R. Kleinrahm, *Densimeters for very accurate density measurements of fluids over large ranges of temperature, pressure, and density.* Metrologia, 2004. **41**: p. S24-S39.
9. McLinden, M.O. and C. Lösch-Will, *Apparatus for wide-ranging, high-accuracy fluid (p, ρ, T) measurements based on a compact two-sinker densimeter.* J. Chem. Thermodyn., 2007. **39**: p. 507-530.
10. McLinden, M.O., R. Kleinrahm, and W. Wagner, *Force transmission errors in magnetic suspension densimeters.* Int. J. Thermophys., 2007. **28**: p. 429-448.
11. McLinden, M.O. and J.D. Splett, *A liquid density standard over wide ranges of temperature and pressure based on toluene.* J. Res. Natl. Inst. Stand. Technol., 2008. **113**: p. 29-67.
12. McLinden, M.O., *Thermodynamic properties of propane. I. p-ρ-T behavior from 265 K to 500 K with pressures to 36 MPa.* J. Chem. Eng. Data, 2009. **54**: p. 3181-3191.
13. Outcalt, S.L. and M.O. McLindent, *Automated Densimeter for the Rapid Characterization of Industrial Fluids.* Industrial & Engineering Chemistry Research, 2007. **46**: p. 8264-8269.
14. Outcalt, S.L., *Calibration Fluids and Calibration Equations: How Choices May Affect the Results of Density Measurements Made with U-Tube Densimeters.* Journal of Research of the National Institute of Standards and Technology, 2018. **123**: p. 123017.
15. May, E.F., et al., *Physical Apparatus Parameters and Model for Vibrating Tube Densimeters at Pressures to 140 MPa and Temperatures to 473 K.* Review of Scientific Instruments, 2014. **85**: p. 095111.

16. Lemmon, E.W., W. Wagner, and M.O. McLinden, *Thermodynamic properties of propane. III. Equation of state.* J. Chem. Eng. Data, 2009. **54**: p. 3141-3180.
17. Meier, K. and S. Kabelac, *Thermodynamic Properties of Propane. IV. Speed of Sound in the Liquid and Supercritical Regions.* J. Chem. Eng. Data, 2012. **57**: p. 3391-3398.
18. Harris, G.L. and J.A. Torres, *Selected laboratory and measurement practices and procedures, to support basic mass calibrations*. 2003, National Institute of Standards and Technology, NISTIR 6969.
19. Richter, M. and M.O. McLinden, *Vapor-phase (p, ρ, T, x) behavior and virial coefficients for the (methane + propane) system.* J. Chem. Eng. Data, 2014. **59**: p. 4151-4164.
20. Span, R. and W. Wagner, *Equations of state for technical applications. I. Simultaneously optimized functional forms for nonpolar and polar fluids.* Int. J. Thermophys., 2003. **24**: p. 1-39.
21. Newell, D.B., et al., *The CODATA 2017 values of h, e, k, and N_A for the revision of the SI.* Metrologia, 2018. **55**: p. L13-L16.
22. Lemmon, E.W. and R.T. Jacobsen, *A new functional form and fitting techniques for equations of state with application to pentafluoroethane (HFC-125).* J. Phys. Chem. Ref. Data, 2005. **34**: p. 69-108.
23. Akasaka, R. and E.W. Lemmon, *Fundamental Equations of State for cis-1,3,3,3-Tetrafluoropropene [R-1234ze(Z)] and 3,3,3-Trifluoropropene (R-1243zf).* Journal of Chemical & Engineering Data, 2019. **64**(11): p. 4679-4691.
24. Akasaka, R. and E.W. Lemmon, *A Helmholtz Energy Equation of State for Calculations of Thermodynamic Properties of trans-1,2-Difluoroethene [R-1132(E)].* Int. J. Thermophys., 2024. **45:** 174**.**.
25. Bell, I.H. and E.W. Lemmon, *Automatic Fitting of Binary Interaction Parameters for Multi-fluid Helmholtz-Energy-Explicit Mixture Models.* J. Chem. Eng. Data, 2016. **61**(11): p. 3752–3760-3752–3760.
26. Bell, I., H., *Mixture Models for Refrigerants R-1234yf/134a, R-1234yf/1234ze(E), and R-134a/1234ze(E) and Interim Models for R-125/1234yf, R-1234ze(E)/227ea, and R-1234yf/152a.* J. Phys. Chem. Ref. Data, 2022. **51**: p. 013103.
27. Goto, T., et al., *Study of decomposition of R-1132(E) as ultra-low GWP refrigerants.* Int. J. Refrig., 2024. **163**: p. 71–77.
28. ECHA, *Annex to the Annex XV Restriction Report; Proposal for Restriction; Version 2*. 2023, European Chemical Agency: https://echa.europa.eu/registry-of-restriction-intentions/-/dislist/details/0b0236e18663449b (accessed May 1, 2024).
29. EPA, *Environmental Protection Agency Fact Sheet: PFAS National Primary Drinking Water Regulation*. 2024: https://www.epa.gov/system/files/documents/2024-04/pfas-npdwr_fact-sheet_general_4.9.24v1.pdf. (accessed September 13, 2024).
30. Solomon, K.R., et al., *Sources, fates, toxicity, and risks of trifluoroacetic acid and its salts: Relevance to substances regulated under the Montreal and Kyoto Protocols.* Journal of Toxicology and Environmental Health, Part B, 2016. **19**(7): p. 289-304.

Supplemental Information

Files for use with the NIST REFPROP database are available at:
https://doi.org/10.6028/NIST.IR.8570sup1

Included in a zip archive are the following ASCII text files:

README.txt	this summary
R1130E.fld	fluid file for R-1130(E), including the EOS presented in Sec. 4.2
R1132E.fld	fluid file for R-1132(E), including the EOS presented in Sec. 4.2
R1234YF.fld	fluid file including the EOS of Lemmon and Akasaka [S1] for R-1234yf used in the fitting of the mixture parameters for the blends containing R-1234yf
HMX.bnc	HMX.bnc file from the standard release of REFPROP v10.0, with the addition of the mixtures contained in the HMX_DOE.bnc file
HMX_DOE.bnc	file containing the mixing parameters fitted in the present project and also mixing parameters from the parallel SERDP-funded project (i.e., the blends listed in Tables 2-2 and 2-3 of the NISTIR.)

The R1130Efld and R1132E.fld files should be added to the “FLUIDS” directory of REFPROP; these pure fluids will then be available upon restarting REFPROP. Note that these may not appear in the list of fluids in the REFPROP GUI (graphical user interface) if the "Refrigerants" fluid set is selected; instead select "All fluids."

The R1234YF.fld file currently in FLUIDS can optionally be replaced with the above file to implement the new EOS; this will yield the values reported in the publications from this project. However, if the user has done extensive work with R-1234yf or blends containing R-1234yf they may want to retain the older version to maintain consistency.

Two versions of the HMX.bnc file (containing the mixture parameters) are provided. Most users should replace the existing HMX.bnc file in the FLUIDS directory with the file provided here.

If, however, you have added mixtures to your HMX.bnc file, or otherwise modified it, you will need to edit your HMX.bnc file to add the mixing parameters given in the HMX_DOE.bnc given here. You will also need to delete the existing entries for: R1234yf/1234ze(E), R1234yf/134a, R134a/1234ze(E), R32/1234yf, R32/1234ze(E), R1234yf/152a, R125/1234yf.

Please be aware, however, that REFPROP v10.0 has a limit of 40 departure functions (these are the "#MXM blocks" in HMX.bnc). The HMX.bnc file in the standard release of version 10.0 contains 27 departure functions, so the additional ones presented here can be accommodated. If the user has added their own custom or proprietary departure functions, it may be necessary to delete ones that are not being used to keep the total at 40 or fewer.

In all cases, please save a backup-copy of any files that you replace or modify.

Supplemental Reference

S1. Lemmon, E. W. and R. Akasaka. An International Standard Formulation for 2,3,3,3-Tetrafluoroprop-1-ene (R1234yf) Covering Temperatures from the Triple Point Temperature to 410 K and Pressures Up to 100 MPa. Int. J. Thermophys., 2022 **43**: 119.